Spectroscopy of Indocyanine Green Photodegradation

Krishna S. Kumar
M.S. Wichita State University 1994

A thesis submitted to the faculty of the
Oregon Graduate Institute of Science & Technology
in partial fulfillment of the
requirements for the degree
Master of Science
in
Computer Science and Engineering

October 1996

The thesis "Spectroscopy of Indocyanine Green Photodegradation" by Krishna S. Kumar has been examined and approved by the following Examination Committee:

Scott Prahl
Assistant Professor
Thesis Research Adviser

Kenton Gregory
Director, Oregon Medical Laser Center

Robert Jaffe
Instructor

Dedication

To my parents

Acknowledgements

I would like to thank the Oregon Medical Laser Center and Dr. Ken Gregory for the lab equipment and support. I would also like to thank the staff and students at OMLC for their support and conversations towards my work and otherwise. Finally, I would like to thank Dr. Scott Prahl for his support and insight into many problems encountered during the course of this work.

Contents

List of Figures

Abstract

Spectroscopy of Indocyanine Green Photodegradation

Krishna S. Kumar, M.S.
Oregon Graduate Institute of Science & Technology, 1996

Supervising Professor: Scott Prahl

In laser tissue welding, indocyanine green (ICG) is topically applied at the weld site to enhance light absorption and to minimize collateral damage. The uptake of ICG by tissues is variable, and photobleaches when exposed to high radiant exposures. To understand these processes, the intimal surface of porcine aorta stained with ICG was exposed to multiple pulses from an 804 nm pulsed diode laser. ICG concentration was varied from 0.8–6.45 mM. Radiant exposures between 20–70 mJ/mm^2 were used with a spot size of 36 mm^2 and a 5 ms pulse duration. After each laser pulse diffusely reflected light from 450–850 nm was obtained from the irradiated spot with an optical fiber based spectrometer. Temperatures were measured during the laser pulse. ICG penetration depth in aorta and the depth of damage were measured. Despite uniform visual appearance, ICG uptake varies by a factor of three at different spots on the same aorta. ICG bleaching is manifested by the shift in absorption peak from 530 nm to 640 nm. The decrease in absorption with successive pulses is an additive effect and follows a power law. The rate of decrease varies linearly with incident energy and may be independent of the concentration of ICG. Temperatures were almost constant with successive pulses. ICG

is absorbed into aorta to a depth of 25 μm but the 804 nm light penetrates to $\sim$15 μm. Strong fluorescence of irradiated samples suggest that some molecular reorganization of ICG occurs.

Chapter 1

Introduction

Laser tissue welding is an emerging surgical technology. It has applications in many surgical specialties and is undergoing a transition from laboratory method to accepted clinical procedure. Laser welding of tissues is a technique that employs the thermal effect of absorbed laser energy to achieve fusion of apposed tissue edges. The various advantages over conventional tissue closure methods such as sutures and staples are that laser welding is faster, has no foreign body reaction, less scar formation, and supports watertight closures.

1.1 History

Laser welding of tissues has been attempted for the last 15 years. The first study of laser effects on blood vessel wall led to the possibility of repairing linear venotomies [1]. In 1979, the first reproducible vascular anastomosis was achieved in rat carotid and femoral arteries with the use of Nd:YAG laser [2]. Later most experiments were conducted with the CO_2 laser because of its availability and familiarity. It has been used for microvessel and nerve anastomoses as well as for joining skin [3–5]. The CO_2 laser's $10.6\,\mu$m wavelength is absorbed strongly by water and has an optical penetration depth of about $13\,\mu$m [6]. Consequently, most of the CO_2 energy is absorbed by the top most layers of the tissue. Therefore, even in a microvessel with wall thickness $\sim 100\,\mu$m, the CO_2 does not provide the uniform heating needed for stable and strong welds. The argon laser with a penetration depth of $\sim 700\,\mu$m at 514 nm produced more uniform heating and

therefore much stronger bonds. It was used successfully for welding structures larger and thicker than microvessels [7–9]. Unfortunately, the anastomoses created were of variable strength due to variations in local tissue thickness, the amount of hemoglobin present, and the state of hydration. Nd:YAG lasers were also used to weld medium-sized vessels due to their higher penetration depths, $\sim$1250 μm at 1.32 μm, but were not as effective as argon lasers which had much better localized heating. Also the 2.15 μm THC:YAG laser [10] and the 1.9 μm Raman shifted Nd:YAG laser with penetration depths of 285 μm and 125 μm respectively, were successfully used to weld microvessels.

1.1.1 Welding Mechanism

Schober's group [11] evaluated electron micrographs of collagen from rat carotid arteries after welding with Nd:YAG laser. They concluded that collagen bonding was responsible for laser welding. It was later suggested that the unravelling of the collagen bundles and the subsequent interaction between these unravelled ends formed a bond [12]. Initially, it was thought that the link formed by the unravelled collagen is a covalent bond [13]. But later experiments strongly suggest that non-covalent bonding is the major mechanism [14, 15]. Though covalent bond formation may take place, it is not necessary for weld strength. Sufficient heat must be generated to denature the protein. The temperatures required to denature all types of collagen is in the range 60–80°C which is essentially the range in which welding occurs [12]. Also it was found that the collagen fibers lost their birefringence at the weld site [12].

1.1.2 Diode lasers and Dyes

CO_2, argon and Nd:YAG laser light is absorbed by the natural chromophores in the tissue for e.g., hemoglobin and melanin in the visible region below 600 nm; by proteins and nucleic acids in the ultraviolet region; and by water in the mid-infrared region. Hence, we are limited by the natural absorption and thermal characteristics of the tissue. The variation of these characteristics can only partially be accounted for by the change in tissue hydration, fat content, pigmentation, thickness, and vascularity. In the spectral

region between 600 and 1300 nm the absorption by most soft tissues is at a minimum. If in this region a photosensitive dye with a known concentration is added to the tissue then the dye with relatively predictable absorption and thermal diffusion characteristics, becomes the primary absorber in this spectral region. These dyes usually have absorption peaks that are matched to the wavelength of the laser used. The energy required for welding is reduced because the light is strongly absorbed by the dye, and consequently a smaller volume of tissue is heated.

Diode lasers can be made much smaller and require less power to operate than gas lasers. Though the semiconductor laser systems have lower peak power output compared to other laser systems, their power output when combined with the energy absorbing dyes is sufficient to weld tissues. One such match for dye-enhanced tissue welding is the readily available 804 nm diode laser and the biocompatible dye Indocyanine Green (ICG). ICG is a water-soluble tricarbocyanine dye initially used for the measurement of cardiac output and is stable in protein-containing solvents [16]. Oz *et al.* [17] used the diode laser and ICG combination to effectively weld abdominal rabbit aorta. They could not achieve welds without the dye. Often these dyes are used with solders and glues for aligning tissues edges to weld anastomoses and fistulas. Fibrinogen-based glues with ICG gives stronger welds but raised concerns over infection risks and handling properties. The need for a clinically usable dye led Bass and his group [18,19] to develop an albumin-based solder that can be doped with ICG producing improved strength and handling characteristics.

1.2 Motivation

Although much time and effort has been spent in bringing laser tissue welding to clinical practice, there are still many gaps in our understanding. What are the physical and optical changes that occur in the tissue during the welding process? What are the laser parameters such as energy density, spot size, and pulse duration for strong and reproducible welds? How are the endpoints of the welding process determined? The

overall goal of this research was to answer such questions and take laser tissue welding closer to clinical reality.

Unlike most welding procedures such as anastomosis and fistulas that are inherently awkward, we place an artificially prepared biomaterial and weld it on top of the tissue. Indocyanine green is topically applied to the tissue and serves as the welding interface. Earlier experiments [20] on the feasibility of welding biomaterial to aorta raised questions about the role of ICG in the welding process. ICG when applied on the tissue penetrates about 25 to 100 μm. Obviously, different penetration depths will be associated with different samples of the same tissue type, but it is not known if the depth is uniform from site to site on a particular sample. It is also not known whether ICG concentration is uniform or decreases as a function of depth.

For pulsed laser welding, ICG layer is bleached and visually changes color from initial green to orange. It is thought that with each laser pulse only a portion of this ICG layer is bleached and thereby changing the effective depth of ICG. In simultaneous transmission and temperature measurements it was found that, though the transmission increased with each pulse there was no change in the temperature recorded. Therefore, the apparent change in the absorption is due to the change in the effective depth of ICG layer which varied as the fourth root of the number of pulses [20]. This same relationship was observed when studying the depth of ocular damage over repetitive pulses of medical lasers [21]. It is not known how a change in concentration of the chromophore or a change in the applied energy density for different concentrations would affect the relation between the depth of damage and the number of pulses. It was also evident from thermal measurements that the temperatures at the surface of the tissue did not change with repetitive pulses. But with the change in effective ICG depth, one would expect the temperatures to change. It is essential to be able to predict the temperatures so that the laser parameters can be set to achieve optimum welds.

The physical changes in the ICG stained layer can be determined by histology but it is invasive and can be done only after the welding process is completed. One of the ways to detect changes non-invasively during welding is to look at remitted light spectrum

from the tissue which could be either transmitted or diffusely reflected light. For clinical investigations it is usually not possible to have the light source and the detector on opposite sides of the tissue, therefore diffusely reflected light from tissue is measured to probe the metabolic and physiologic status of the tissue. Additionally, this method can be totally fiber-based and hence can be used endoscopically and via catheters.

More specifically, reflectance experiments will be carried out to understand the spectral changes of ICG layer with laser pulse. Thermal experiments, to correlate to the temperature predicted by reflectance measurements and finally, histology to measure the depth of penetration of ICG.

Chapter 2

Materials and Methods

To assess changes in indocyanine green following laser irradiation, spectroscopic, thermal and histologic measurements of the ICG stained tissues were made. The main objective of this work was to understand how indocyanine green is affected by each laser pulse.

2.1 Sample Preparation

Porcine aorta was used in all the experiments. Frozen aorta was thawed to room temperature and kept moist to prevent dehydration. The thawed aorta was cut in square pieces with a surface area of approximately $4\,\mathrm{cm}^2$. A few drops of freshly prepared stabilized indocyanine green [Sigma Chemical Co.] solution with concentrations from 0.8–6.5 mM was topically applied on the intimal surface of aorta and let stand for 2–3 minutes after which the remaining solution on the tissue was dabbed away. Optical density of indocyanine green (ICG) in aqueous solution declines rapidly in the first few minutes [16]. Therefore it was stabilized by adding 25% human serum albumin before ICG was applied on the tissue. ICG is absorbed in the tissue and forms the target layer during laser exposure Figure 2.1.

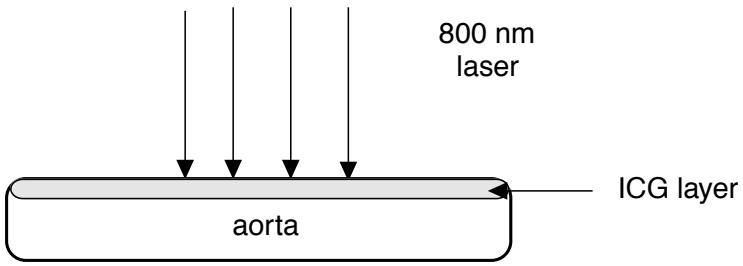

Figure 2.1: ICG topically applied on aorta forms a layer that is irradiated with the laser.

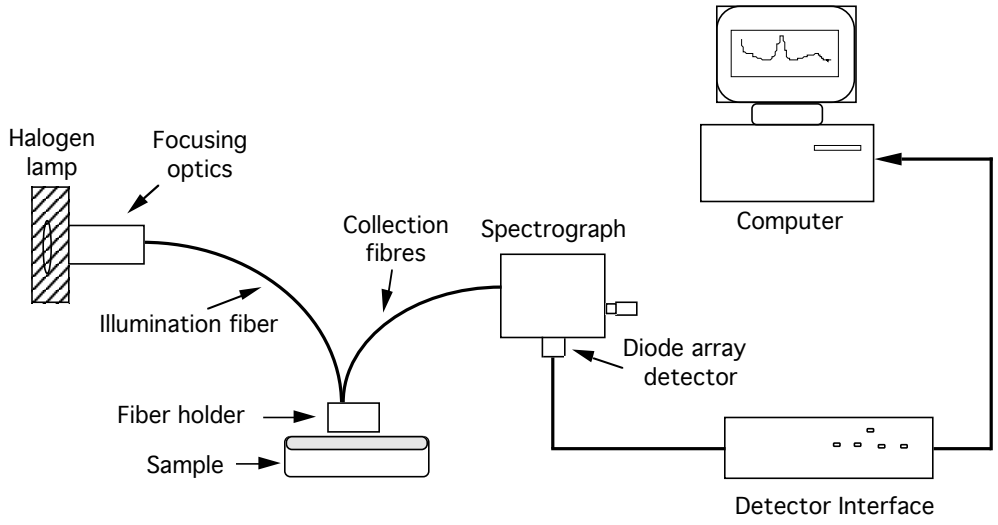

Figure 2.2: Schematic of the experimental setup.

2.2 Reflectance Spectroscopy

Figure 2.2 is a schematic of the optical measurement system used to measure the diffusely reflected light from the tissue. The light source was a 100W quartz-tungsten-halogen lamp [Model 6333 Oriel Instruments] that is focused onto one end of the bifurcated fiber bundle. The illumination arm of the bifurcated bundle consists of a single 1 mm diameter fiber located in the center (Figure 2.3). Six fibers are used to collect the light. One end of the fiber bundle is fixed in an aluminum fiber holder, Figure 2.2, at an angle of about 20° from the normal to the tissue surface. This ensures that the illuminating and collecting fibers are always at a fixed distance from the surface, facilitates easier handling of the bundle, and more importantly eliminates the specularly reflected light from the tissue (Figure 2.2). The collected light is transmitted to a spectrograph [Model 1229 EG&G] with a 25 μm slit.

The spectrograph with a focal length of 156 mm has a 300 grooves/mm grating for dispersing the light onto an array detector with 1024 silicon photodiodes [Model 1453A EG&G]. The resolution was about 0.5 nm/detector using the 25 μm slit. The full detection spectrum was about 500 nm broad. A detector interface [Model 1471A EG&G] has a

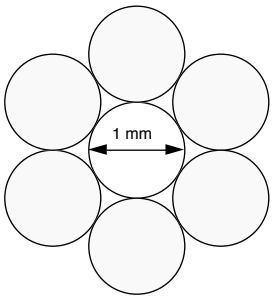

Figure 2.3: The fiber bundle used for light delivery consists of one central illuminating fiber surrounded by six detection fibers (shaded). The fiber diameter was 1 mm with a core diameter of 300 μm.

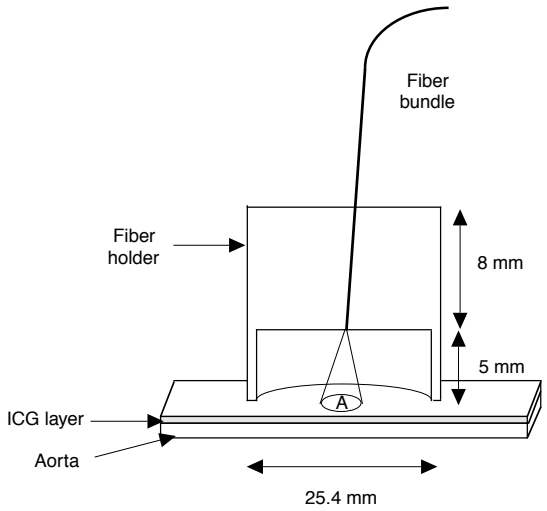

Figure 2.4: Front view of fiber bundle placed in the holder. The area A illuminated is about 20 mm^2.

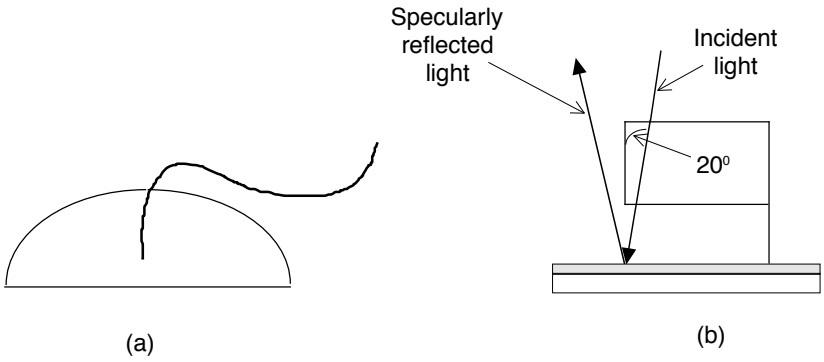

Figure 2.5: (a) Top view of the holder (b) Side view showing the escape of specularly reflected light.

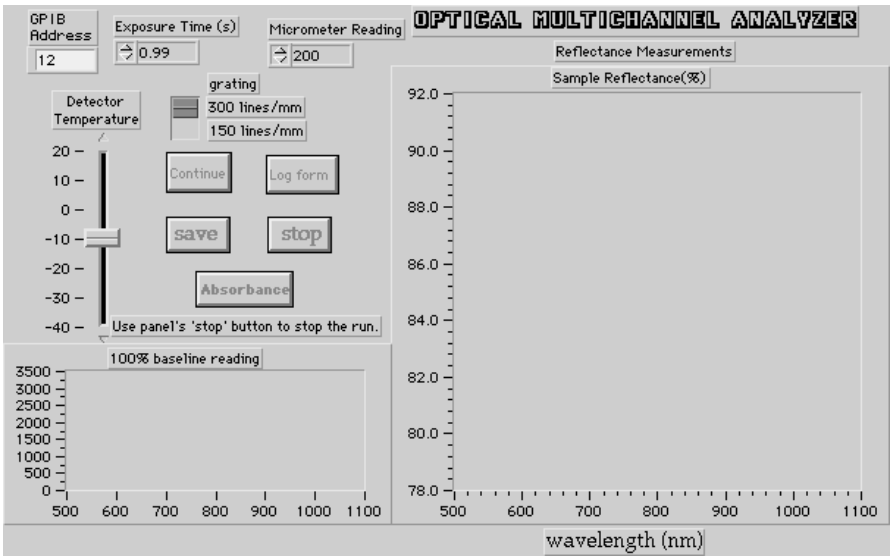

Figure 2.6: Optical Multichannel Analyzer control panel

15 bit A/D conversion range giving a full-scale count upto 32,767 and permitted communication between the computer and the detector. The interface is a microprocessor-based data acquisition system that can collect, store, and preprocess spectral data under the control of a host computer. LabView software was used to control the interface unit.

2.2.1 Virtual Optical Multichannel Analyzer

An optical multichannel analyzer (OMA) virtual instrument was developed using the LabView software to drive the interface. The control panel of the OMA is shown in Figure 2.6. The OMA facilitates the operation of the detector and interface, real-time data acquisition, analysis, and graphical representation. A flowchart of OMA operation is shown in Figure 2.7.

The initial input values to the OMA are the GPIB address of the detector interface, the temperature to which the detector is to be set, the number of grooves per mm of the diffraction grating, the micrometer setting of the spectrograph, and the time over which the collected data is to be averaged. The OMA calculates the range of the spectrum to be displayed from the micrometer setting. Calibration of the OMA was done using a Hg

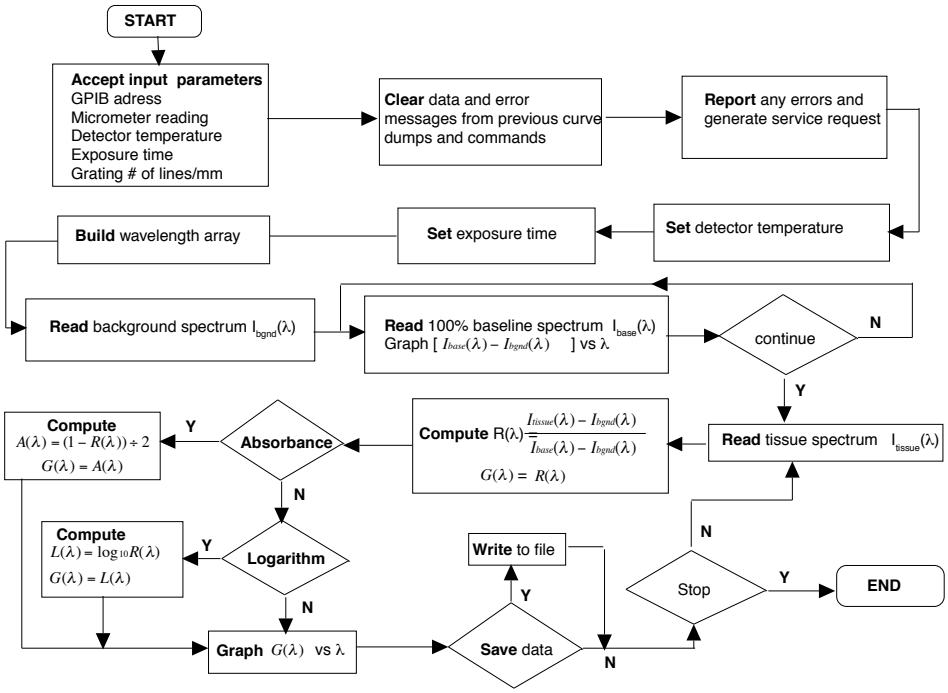

Figure 2.7: Flowchart of OMA's execution sequence

lamp. The procedure is as follows,

- A Hg lamp spectrum was recorded using the OMA in a spreadsheet form.
- Pixel numbers (n) of Hg lamp's emission peaks were noted using spreadsheet columns between the numbers 1 - 1024.
- From manufacturers [Oriel] data the peak emission wavelengths of Hg lamp were obtained.
- The difference between adjacent peaks Δn, in terms of pixel numbers (n) and the difference $\Delta\lambda$, in terms of wavelength (λ) were calculated.
- Increment $Inc = \Delta\lambda/\Delta n$ were computed for all the peaks to get pixel increments in terms of nm /pixel. An average increment was then calculated.

- The wavelength λ of the first pixel = Some peak's wavelength λ - (that peak's n * Inc)
- Offset was set accordingly.

The OMA first collects the background spectrum $I_{bgnd}(\lambda)$, that is the detected signal when the source lamp is off. A baseline measurement is made on a glass slide with three coats of Krylon white paint and the lamp on. This is the 100% baseline signal $I_{base}(\lambda)$. The tissue sample is placed on this white glass slide to obtain the tissue measurement, $I_{tissue}(\lambda)$. The measured reflectance is calculated as,

$$R(\lambda) = \frac{I_{tissue}(\lambda) - I_{bgnd}(\lambda)}{I_{base}(\lambda) - I_{bgnd}(\lambda)} \tag{2.1}$$

The reflectance of the tissue versus wavelength range is displayed and updated every acquisition interval. The displayed data may be saved at any time for further analysis. Initially, a reference reflectance measurement $R_{ref}(\lambda)$ of unstained aorta is made and all measurements of stained aorta $R_{stain}(\lambda)$ are normalized to this reference measurement, such that the normalized reflectance

$$\rho(\lambda) = \frac{R_{stain}(\lambda)}{R_{ref}(\lambda)} \tag{2.2}$$

The reflectance of the stained tissue was normalized to that of unstained tissue to remove any intrinsic absorption peaks of the tissue due to its natural chromophores and to express the reflectance of unstained tissue as 100% reflectance. It is not known if indocyanine green, when applied on aorta, is absorbed uniformly or if there is a gradient with decreasing absorption as the depth z increases. But a photon that is diffusely reflected from the layer does not carry information about absorption at a particular depth instead contains the average absorption properties over the thickness of the material that it has travelled. Defining optical depth $\tau(\lambda)$ as the average product of depth z and absorption coefficient $\mu_a(z)$ at that depth, we can write Beer's law as,

$$\rho(\lambda) = \exp\left[-\frac{2}{d}\int_0^d z\mu_a(z)dz\right] \tag{2.3}$$

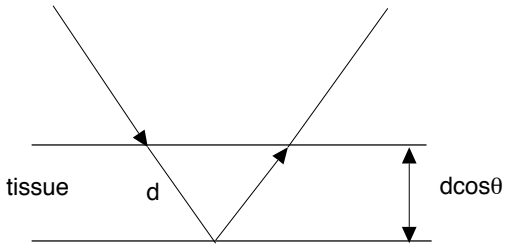

Figure 2.8: Light path travelling through the thickness of the layer twice

The above equation holds because the stained layer is assumed to absorbing only and its thickness is of the order of a few microns. It is essentially like adding an absorbing filter (Figure 2.1). The factor 2 comes from the fact that the diffusely reflected light traverses the thickness of the layer twice (Figure 2.8). From the above equation the optical depth $\tau(\lambda)$ is,

$$\tau(\lambda) \equiv \frac{1}{d}\int_0^d z\mu_a(z)dz = -\frac{1}{2}\ln\rho(\lambda) \tag{2.4}$$

2.2.2 Effect of source lamp on ICG

To understand how intensity of light from the halogen lamp degrades ICG, an aorta sample was prepared with 6.45 mM ICG solution and was exposed to 0.1 $\mathrm{W/cm^2}$ light for about 90 minutes at one spot. Reflectance measurements of the spot being exposed were taken immediately on placing the fiber-holder on the tissue sample and after 2, 4, 6, 8, 10, 15, 20, 30, 70, and 90 minutes to see any changes in the absorption characteristics

of ICG.

2.2.3 Variable uptake of ICG

When ICG is deposited topically on the surface of the tissue, ICG is absorbed, and the surface of the tissue looks uniformly green to the eye. It is assumed that ICG is absorbed in such a way that it forms a layer of uniform thickness. To measure any site to site non-uniformities in this layer, two samples were prepared with 6.45 mM ICG concentration. On one sample single reflectance measurements were taken at 8 different spots covering the whole tissue surface. And on the second sample reflectance measurements were taken thrice on a spot. This was repeated at five different spots on the tissue sample.

2.2.4 Concentration Variation

When the ICG layer is subject to pulsed laser light, the transmission of the tissue increases with each pulse [20]. This means that either the absorption coefficient of ICG decreases with each pulse or the thickness of the ICG layer decreases as ICG is bleached with each pulse or both absorption coefficient and the thickness decrease together.

To evaluate the earlier transmission experiments using reflectance techniques were used with multiple ICG staining concentrations. The average absorption coefficient or thickness of ICG layer was measured after each laser pulse. Two sets with 3 aorta samples each were prepared for staining. The three samples of the first set were stained with ICG at concentrations of 0.8, 3.2, and 6.45 mM and subjected to radiant exposure of 40 mJ/mm^2. A 36 mm^2 spot size was used. The three samples of the second set were stained with 0.8, 1.6, and 6.45 mM concentrations of ICG and subjected to radiant exposure of 20 mJ/mm^2 from the diode laser. The pulsed diode array laser [Star Medical Technologies] operated between 790–810 nm. ICG when bound to albumin has peak absorbtions at 730 nm and 805 nm [22]. A pulse width of 5 ms and a spot size of 0.36 cm^2 were used. Each sample was subjected to 4–6 pulses from the diode laser and reflectance measurements were taken after each pulse.

2.2.5 Energy Variation

These set of experiments were performed as a continuation of the above experiments to understand how the ICG absorption and thickness of the layer changes with each laser pulse of different incident energy. Four samples stained with 6.45 mM ICG were prepared and subjected to radiant exposures of 28, 42, 55, and 70 $\mathrm{mJ/mm^2}$ each. Again a pulse width of 5 ms and a spot size of 0.36 $\mathrm{cm^2}$ were used. Each sample was irradiated with 10 pulses from the laser and reflectance measurements were taken after each laser pulse.

2.3 Thermal Radiometric Experiments

When tissue stained with ICG is irradiated with a pulsed laser it was seen that the temperatures at the surface of tissue remained constant for each pulse [20]. Reflectance measurements indicate that the optical depth decreases with each laser pulse. When a tissue with an absorption coefficient of μ_a is subject to radiant exposure of Φ ($\mathrm{J/cm^2}$) then the temperature (neglecting thermal diffusion and scattering) is,

$$\Delta T = \frac{\mu_a \Phi}{\varrho c} \tag{2.5}$$

where ϱc is the heat capacity of the tissue. Optical depths ($\tau = \mu_a d$) extracted from reflectance measurements are proportional to temperature. Therefore if optical depth decreases with each pulse so should the temperature. Using the non-invasive technique of pulsed photothermal radiometry one can measure the surface temperatures and the internal thermal profiles can be extracted from the measured surface temperatures [23, 24]. These experiments were done to correlate thermal and reflectance measurements.

Thermal measurements of aorta stained with 6.45 mM ICG solution were made using a mercury-cadmium-telluride (HgCdTe) infrared detector. A schematic of the experimental setup is shown in Fig 2.9. The HgCdTe photoconductive detector (EG&G Judson) is sensitive from 8–12 μm, with a peak sensitivity at 11 μm. The active detector area is 1 $\mathrm{mm^2}$ and has a field of view of 60°. The optics focuses a 1 $\mathrm{mm^2}$ spot from the sample

to the active detector. The detector operates at 77 K and is cooled by liquid nitrogen. A low noise impedance-matched pre-amplifier with a variable gain and a bandwidth of 1.5 MHz amplified the signal from the detector. The laser used was the 800 nm pulsed diode laser and a pulse width of 5 ms. The laser head and the detector were placed at an angle of 45° from the normal to the surface of the sample and 90° from each other. The detector was 5 cm away from the sample whereas the laser was 1 cm away. A surface temperature profile was recorded on the oscilloscope during and after the laser pulse. Two aorta samples were prepared with 6.45 mM ICG solution. The first sample was subjected to radiant exposures of 66 mJ/mm^2 and surface temperatures were measured for 20 consecutive pulses. The second sample was subjected to radiant exposures of 33 mJ/mm^2 for 20 pulses. Surface temperatures were measured and also a diffuse reflectance measurement of the sample was taken each time before the sample was irradiated. The detector was initially calibrated with a 5 mm aperture using a black painted aluminum block as a black body. The response of the detector at different temperatures was calibrated with temperature measurements of the black body by a thermocouple.

2.4 Histologic assessment

From reflectance measurements optical depths can be extracted, but to quantify the change in absorption coefficient direct measurements of ICG penetration depth and the depth of damage due to irradiation had to be performed. Histologic assessments of irradiated tissue samples were made to measure ICG penetration depth and to understand how depth of damage to the tissue varies with each laser pulse. It is expected that these measurements correspond to the decrease in optical depth seen from reflectance measurements. Ten samples stained with 6.45 mM ICG solution were prepared. The first sample was irradiated with one laser pulse, the second sample with two and so on upto ten pulses on the tenth sample. The pulsed diode laser with a pulse width of 5 ms and a radiant exposure of 55 mJ/mm^2 was used. Reflectance measurements were made on each sample after each pulse. Then the samples were sectioned and examined under a

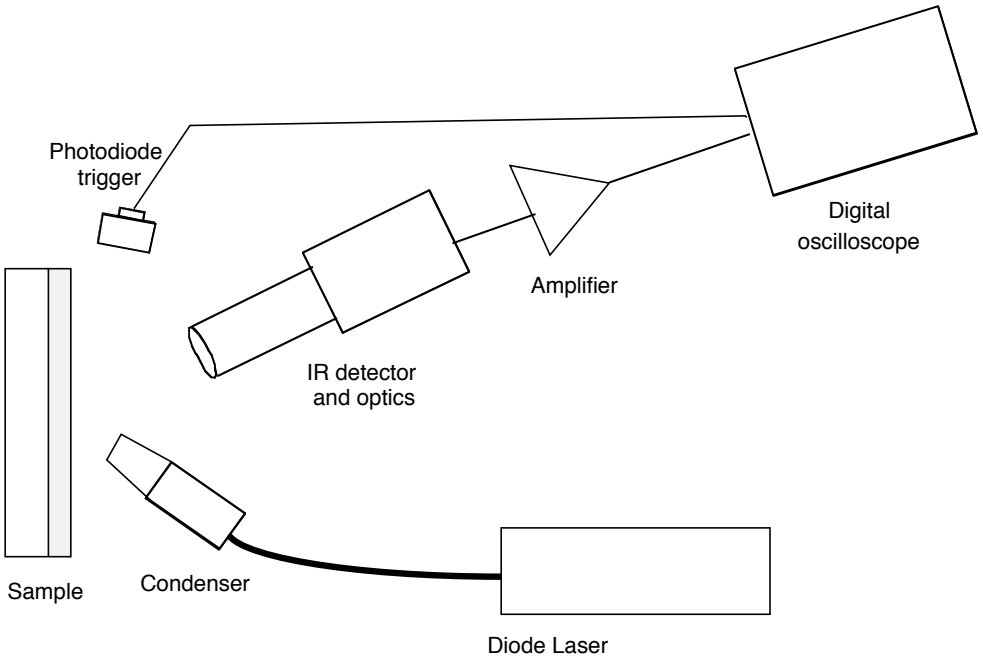

Figure 2.9: Experimental setup for thermal measurements

fluorescence microscope using a 470–490 nm excitation source. The thickness of the ICG layer was measured before irradiating with laser and thickness of the bleached layer of each sample was also measured. Photographs of all the samples were taken.

Chapter 3

Results

The results from the reflectance, thermal and histological measurements are presented in this chapter. Reflectance measurements indicated indocyanine green's degradation with light exposure.

3.1 Reflectance Spectroscopy

3.1.1 Virtual Optical Multichannel Analyzer

Following the calibration procedure described in Chapter 2, the peak wavelengths of the Hg lamp and the respective pixel numbers are given in Table 3.1 for a micrometer setting of 150.

Table 3.1: Mercury lamp emission peaks and the positions of the peaks along the photodiode array

Peak Wavelength(nm)	Pixel Number	Slope nm/pixel
404.6	180	
435.8	239	0.528
546.1	444	0.538
576.9	503	0.522
	Average =	0.529 ± 0.008

Doing the calculations for the first two adjacent peaks, $\frac{435.8-404.6}{239-180} = 0.529\,\text{nm}$ /pixel. Repeating the procedure for all the peaks an average of 0.529 nm /pixel was obtained.

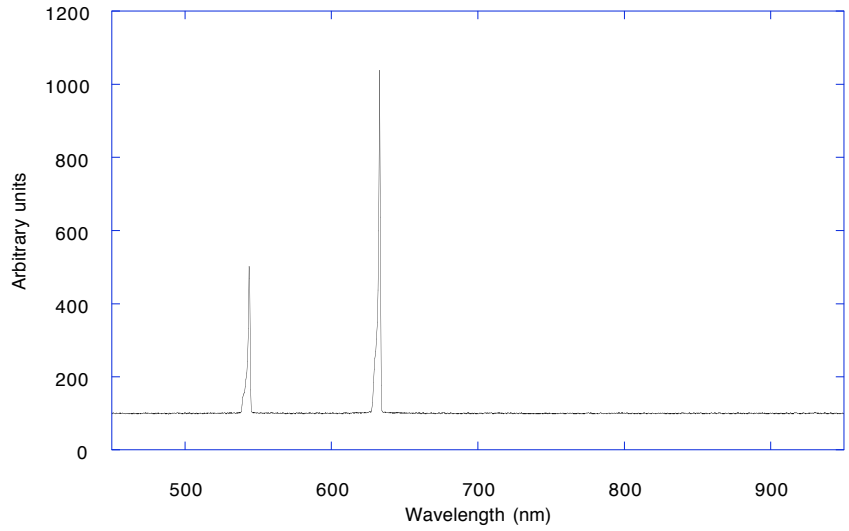

Figure 3.1: Spectrum of green and red Helium-Neon lasers obtained using the calibration

This value is the resolution of the spectrograph/detector. This gives a value of 309 nm for the first pixel and the offset is about -291 nm. Figure 3.1 shows the spectrum from green and red HeNe lasers obtained from using the above calibration values. Figure 3.2 shows a reference reflectance spectrum of unstained aorta $R_{ref}(\lambda)$ and a spectrum of aorta stained with ICG $R_{stain}(\lambda)$. Figure 3.3 shows the normalized spectrum $\rho(\lambda)$. It can be seen in the normalized spectrum that the absorption peaks due intrinsic tissue absorption are not present. The normalized spectrum only includes changes induced by the addition of ICG to the tissue.

3.1.2 Effect of source lamp on ICG

Figure 3.4 shows the changes in the stained ICG layer on aorta as the layer is constantly exposed to the halogen lamp over a period of 90 minutes. The irradiance is about 0.1 W/cm^2. The peak initially at around 540 nm shifts to 600 nm. The broad absorption between 660–850 nm slowly starts to narrow and an absorption peak at 800 nm appears at the end of 2 hours. The first spectrum was obtained immediately on placing

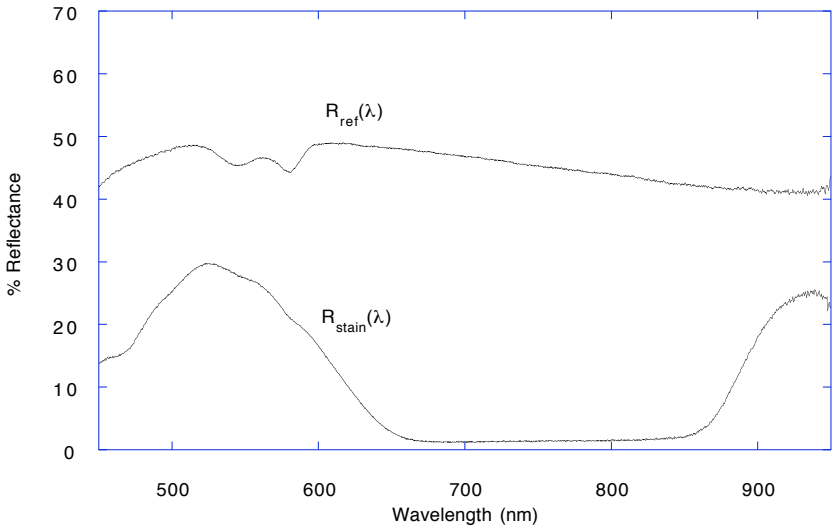

Figure 3.2: Spectra of unstained aorta R_{ref} and aorta stained with ICG R_{stain}. Absorption peaks due to blood are seen at 542 and 577 nm

the fiber-holder on the sample and the second spectrum after 6 minutes. The spectral characteristics do not change much in this time. The OMA updates the spectrum every second and it takes not more than 10 seconds to position the fiber-holder on the tissue sample and to obtain a spectrum. Therefore it is assumed that in this 10 seconds the light from the lamp did not significantly affect any spectral changes in the ICG layer of the sample.

3.1.3 Variable uptake of ICG

The variation in the diffuse reflectance at 8 different spots on the first aorta sample can be seen from Figure 3.5. The variation is only in the overall magnitude of the reflectance that varies by about a factor of three. Figure 3.6 shows the variation in the diffuse reflectance at one spot on the second sample. Three separate reflectance measurements were made on a single spot. Each time the fiber-holder was removed and replaced as close to the same spot as possible. The variation is probably because

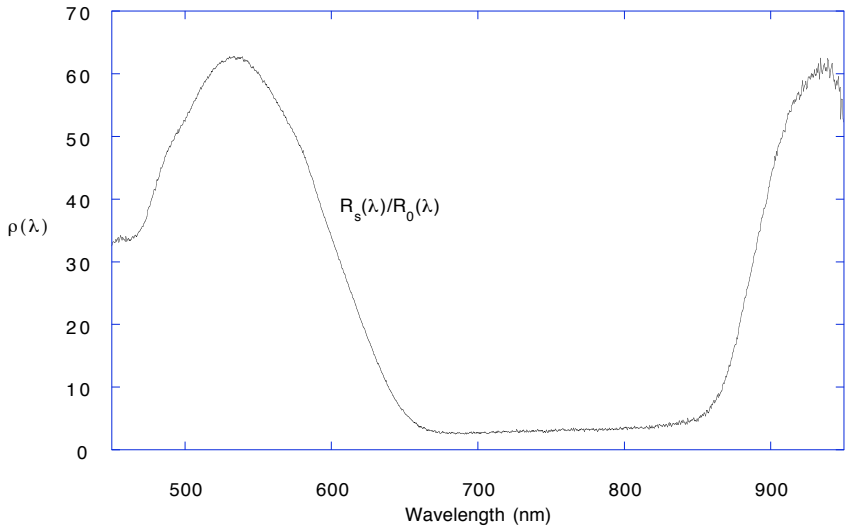

Figure 3.3: Normalized reflectance spectrum. Normalization removes all intrinsic tissue absorption, and indicates the changes in reflection caused by ICG staining.

the exact same spot area was not covered. Figure 3.7 shows the average of these three reflectance measurements at five different spots on the tissue. Again the reflectance varied at least by a factor of three.

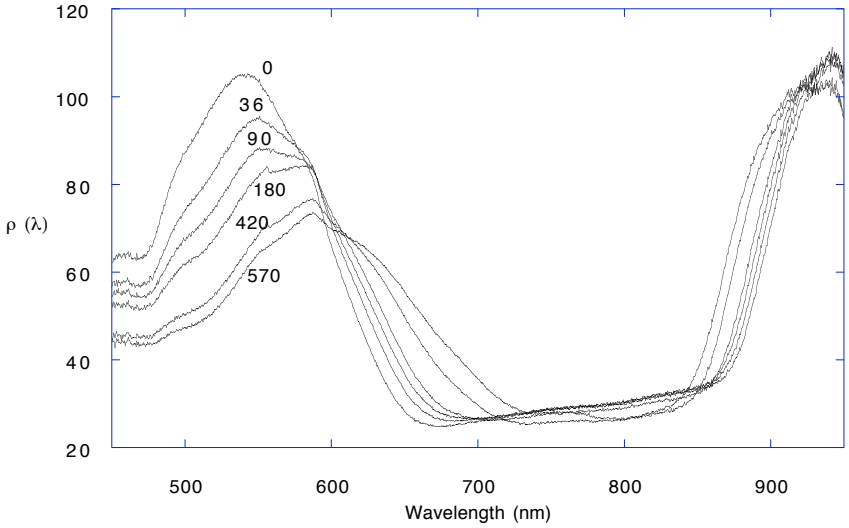

Figure 3.4: Degradation of ICG with increasing radiant exposures (J/cm^2) from the halogen lamp source. The irradiance was $0.1\,W/cm^2$ and ICG concentration was 6.45 mM.

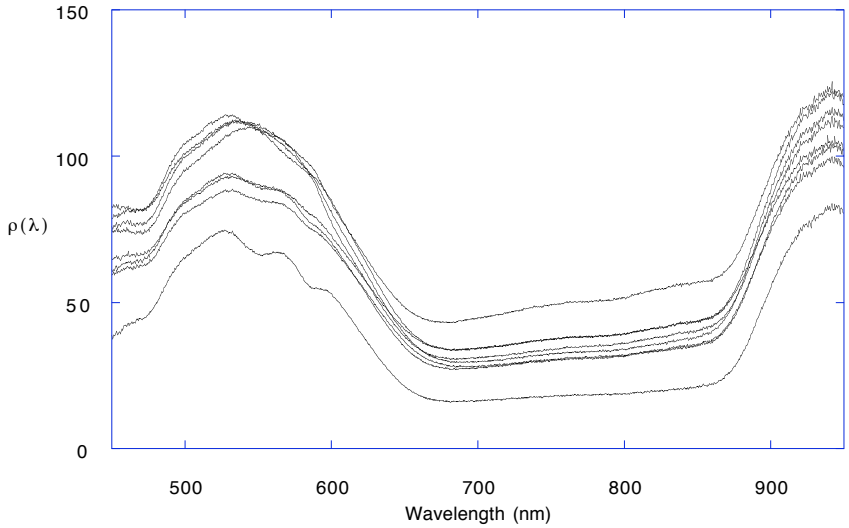

Figure 3.5: Variation in diffuse reflectance along the ICG layer at 8 different spots on the sample. Concentration of ICG was 6.45 mM.

3.1.4 Concentration variation

The diffuse reflectance of tissue samples stained with ICG solution changes with each pulse from the diode laser. Figures 3.8, 3.9, and 3.10 show the changes in samples stained with 6.45, 3.2, and 0.8 mM ICG respectively. These three samples were subjected to radiant exposure of 40 mJ/mm^2. In figure 3.8, the reflectance before any exposure to the laser has a peak at around 530 nm. This peak corresponds to the visual green coloration of the ICG layer. There is also the broad absorption between 660–860 nm. With each laser pulse, the peak initially at 530 nm shifts to longer wavelengths. After 6 pulses the peak is around 640 nm. This phenomena, termed bleaching, is seen visually as the color of the ICG layer changes from green to bright orange.

The broad absorption from 660–860 nm starts to narrow with each pulse. By the fifth pulse two individual absorption peaks begin to appear. The initial broad absorption between 660–860 nm that is seen before irradiation could be due to unresolved, overlapping absorption bands. After a few pulses the absorption decreases, and the instrument is able to resolve features in the spectrum. Similar trends are seen in Figure 3.9 for the sample stained with 3.2 mM ICG solution. For a much lower concentration of 0.8 mM, the two individual peaks can be seen in Figure 3.10 at 740 and 800 nm respectively, before and after irradiation. Though reflectance increases gradually there is no bleaching.

The diffuse reflectance measurements for the second set of samples are shown in figures 3.11, 3.12 and, 3.13. These samples were irradiated with 20 mJ/mm^2 radiant exposure. Even for the sample with highest concentration of 6.45 mM ICG, only faint bleaching can be seen in Figure 3.11 due to the small shift in the peak from 540 nm to 560 nm. No visually discernable change in color was seen in this sample. In the other two samples stained with 1.6 and 0.8 mM ICG solution (figures 3.12, 3.13), bleaching is not seen but reflectance increases slowly with each pulse.

3.1.5 Energy variation

Noting the difference in the previous section between samples stained with similar ICG concentrations but irradiated with different radiant exposures, reflectance measurements were made on samples prepared with one ICG concentration of 6.45 mM and four different energies. The resulting diffuse reflectance after each pulse can be seen in figures 3.17, 3.16, 3.15, and 3.14 for radiant exposure of 28, 42, 55, and 70 mJ/mm^2 respectively. With increasing energy, ICG bleaches with fewer pulses and also the reflectance increases more rapidly. A reflectance of more than 70% beyond 900 nm after a few pulses indicates that the reflectance of stained tissue may exceed that of unstained unirradiated tissue and may be associated with cooking of the tissue.

3.2 Thermal Radiometric Experiments

The calibration of the thermal detector is shown in figure 3.18. Without an aperture the detector saturated for temperature rises of 50°C, therefore it was calibrated with a 5 mm aperture that extended its range to 240°C. The detector response was linear for a temperature rise of upto 50°C with an increase of 15 mV/°C. The surface temperatures of the first sample irradiated with 20 pulses of 66 mJ/mm^2 as shown in Figure 3.19. The temperatures were almost a constant for all 20 pulses. The average temperature rise was about 35 ± 2°C. The surface temperatures of the second sample for 20 pulses of 33 mJ/mm^2 each is shown in Figure 3.19. The average temperature rise is 14 ± 1°C. Diffuse reflectance measurements made on the sample before and after 5, 6, 10, 15 and 20 pulses is shown in Figure 3.20. A small 1 mm diameter bleach spot appeared on the tissue after 5 pulses. After 20 pulses the spot size was about 10 mm^2. Bleaching is also evident from the reflectance measurements.

3.3 Histologic assessment

Thickness measurements of ICG layer on stained internal elastic lamina of porcine aorta shows that the layer is about 25–50 μm thick. A 10–15 μm darkly stained layer is followed by a gradually lightening stain layer that may extend upto 50 μm. Thickness measurements for samples irradiated with progressive number of pulses made under fluorescence microscopy showed a clear fluorescing layer of 10–15 μm. The thickness of this layer never increased significantly with successive pulses, though fluorescence seemed to increase in brightness with each pulse. Photographs of the ICG fluorescence were taken at magnification 10×. Figure 3.21 shows the intimal surface of aorta stained with 6.45 mM ICG solution. The thickness of the stain layer was 25–30 μm. In Figure 3.22, a bright fluorescing portion of the irradiated layer is seen on the right and a faintly fluorescing portion on the left is the unirradiated control. Figures 3.23, 3.24, 3.25, and 3.26 show the fluorescing layer of samples irradiated with 1, 2, 5, and 10 pulses respectively. The radiant exposure was 55 mJ/mm^2 per pulse and all the samples were stained with 6.45 mM ICG. Reflectance measurements were made on all the samples. Figures 3.27 and 3.28 are diffuse reflectances of samples irradiated with 66 mJ/mm^2 for 1 and 10 pulses respectively. All samples bleached with the first pulse. Aorta stained with ICG fluoresces and upon irradiation fluoresces more strongly.

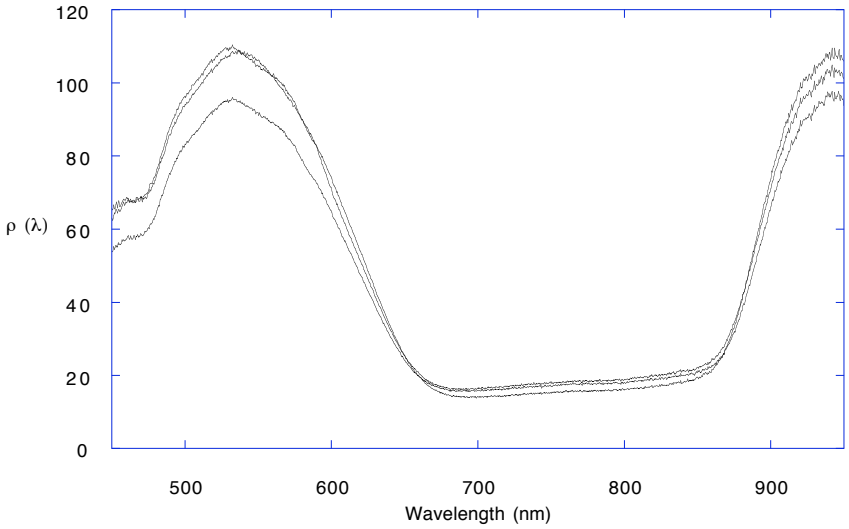

Figure 3.6: Diffuse reflectance measured at approximately the same spot three times on tissue stained with 6.45 mM ICG solution.

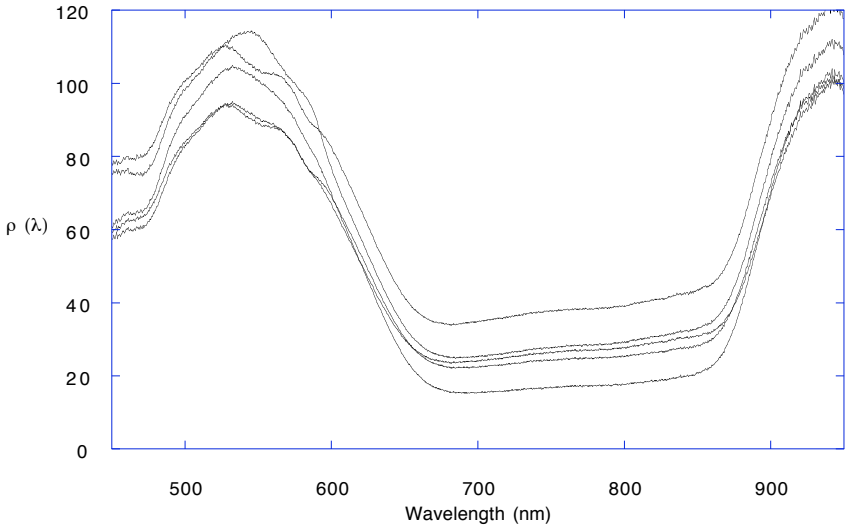

Figure 3.7: Diffuse reflectance at five different spots each averaged over 3 measurements.

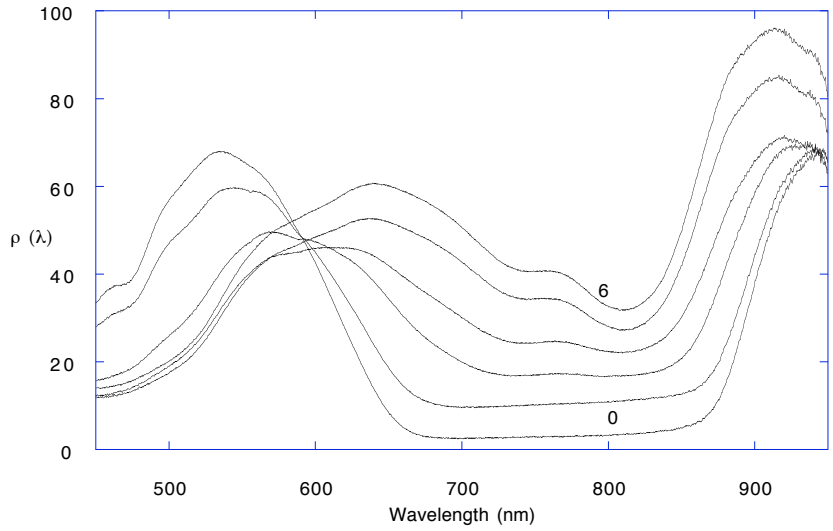

Figure 3.8: The change in diffuse reflectance with each pulse. The sample was stained with 6.45 mM ICG and irradiated with 40 mJ/mm^2. The peak moving from 530 nm to 640 nm represents visible bleaching.

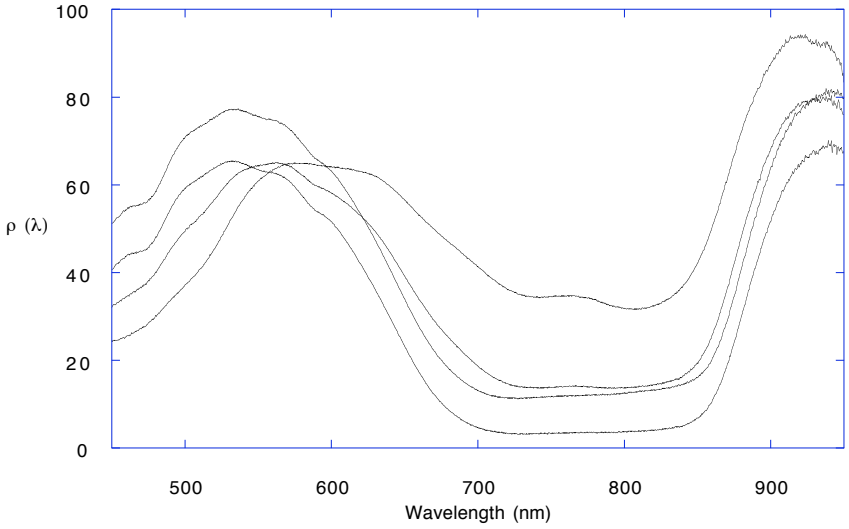

Figure 3.9: The change in diffuse reflectance with each pulse. The sample was stained with 3.2 mM ICG and irradiated with 40 mJ/mm^2.

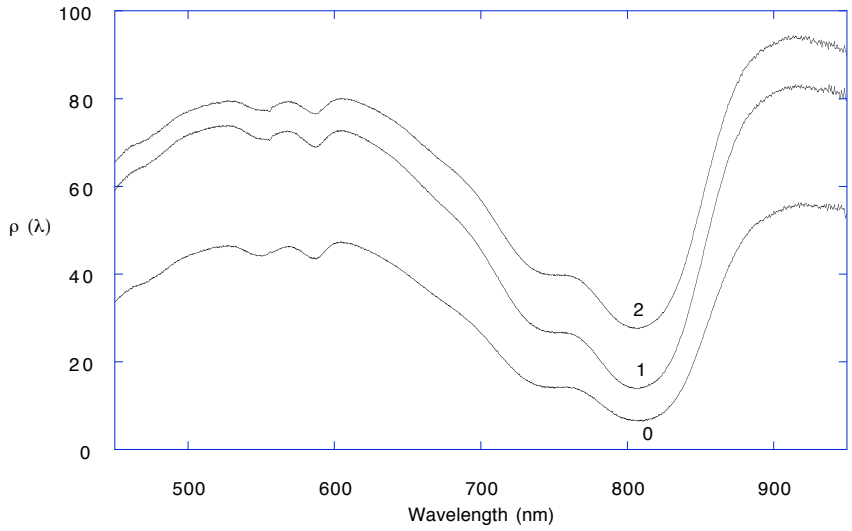

Figure 3.10: The change in diffuse reflectance of a sample stained with 0.8 mM ICG and irradiated 40 mJ/mm^2. Bleaching does not take place at this low concentration of ICG

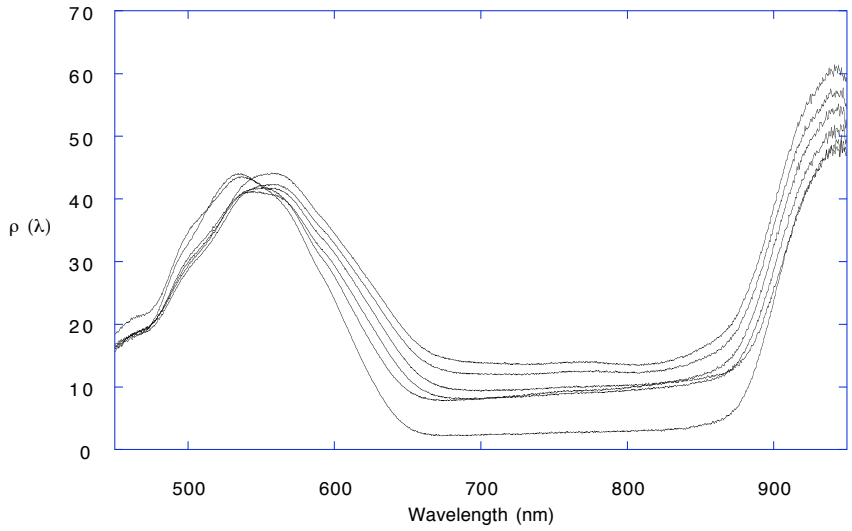

Figure 3.11: Diffuse reflectance of sample stained with 6.45 mM ICG and irradiated 20 mJ/mm^2. A shift in peak from 540 to 560 nm is evident from the spectrum, though visually detectable change in color was not observed.

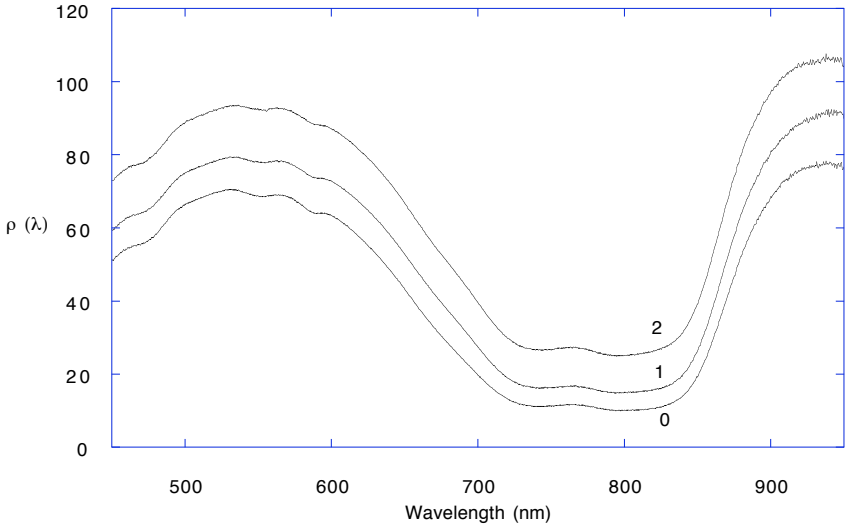

Figure 3.12: Diffuse reflectance of a sample stained with 1.6 mM ICG and irradiated with 20 mJ/mm^2.

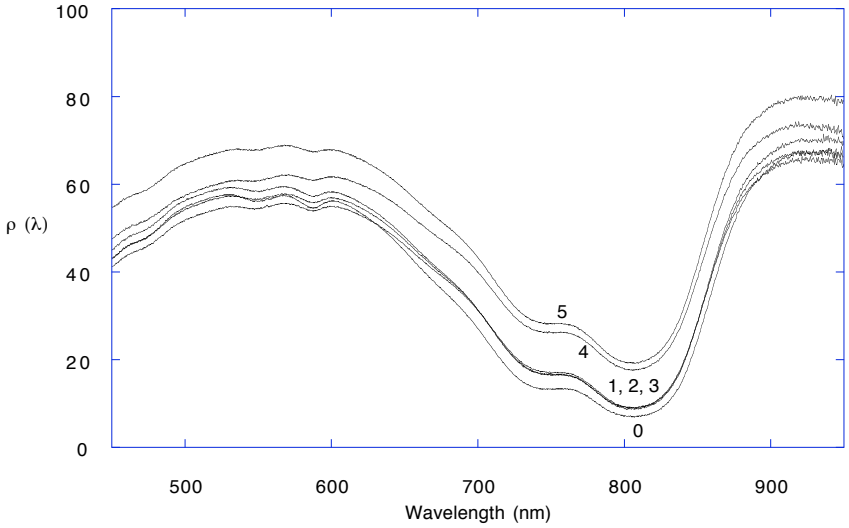

Figure 3.13: Diffuse reflectance of a sample stained with 0.8 mM ICG and irradiated with 20 mJ/mm^2.

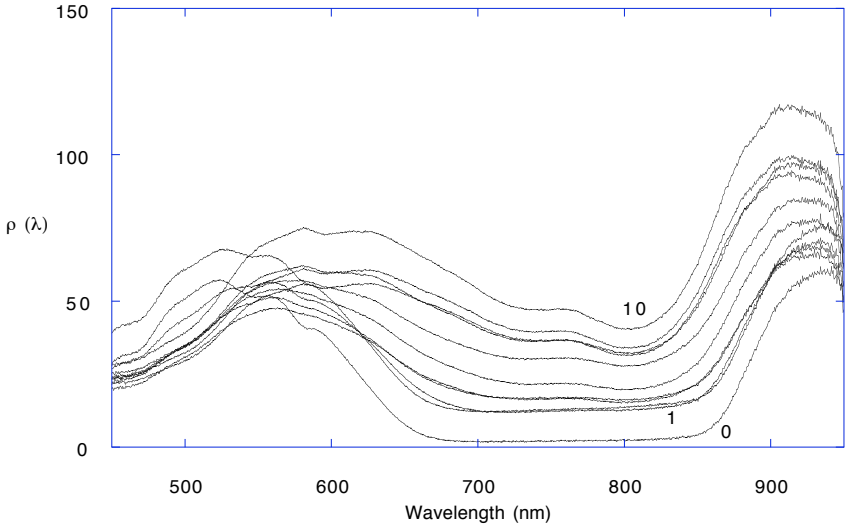

Figure 3.14: The diffuse reflectance of a sample irradiated with radiant exposures of $28\,\mathrm{mJ/mm^2}$ and stained with 6.45 mM ICG solution.

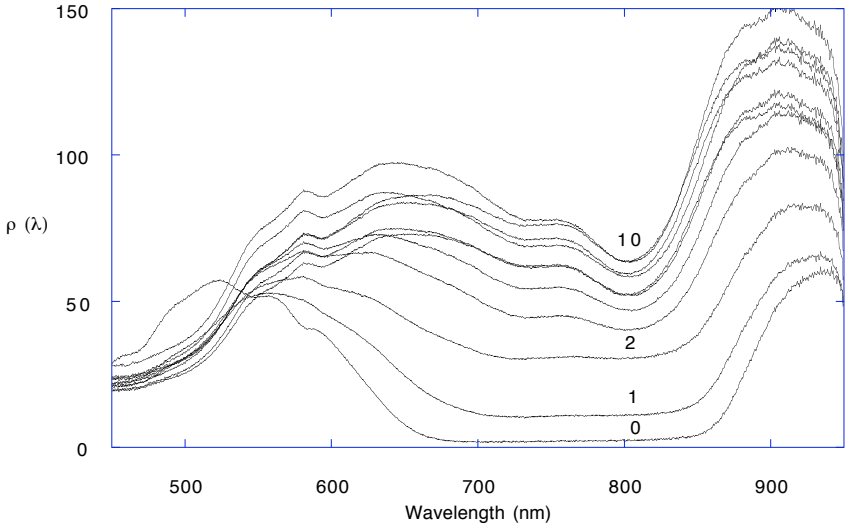

Figure 3.15: The diffuse reflectance of a sample irradiated with radiant exposures of $42\,\mathrm{mJ/mm^2}$ and stained with 6.45 mM ICG solution.

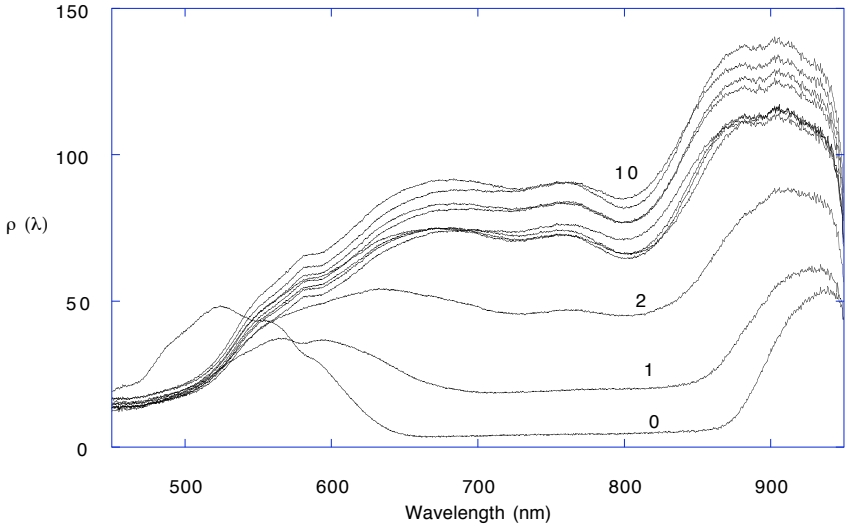

Figure 3.16: Diffuse reflectance measurements of sample irradiated with radiant exposures of 55 mJ/mm^2 and stained with 6.45 mM ICG solution.

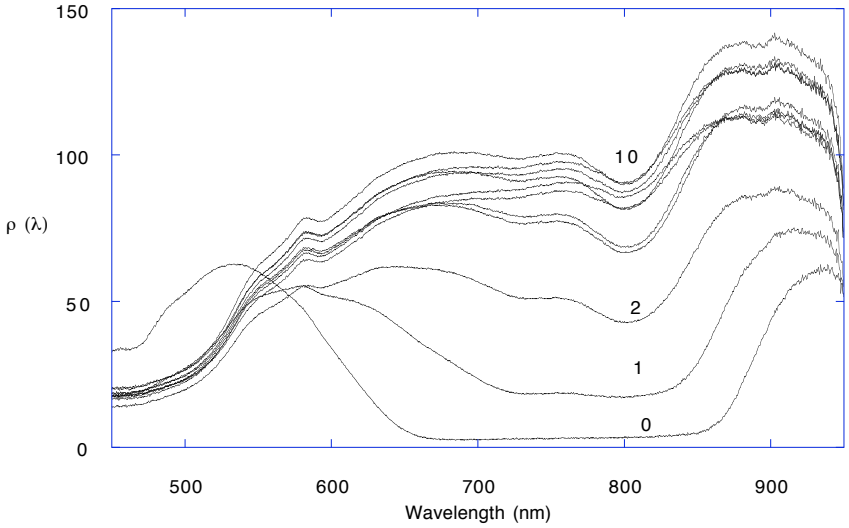

Figure 3.17: Diffuse reflectance measurements of sample irradiated with radiant exposures of 70 mJ/mm^2 and stained with 6.45 mM ICG solution.

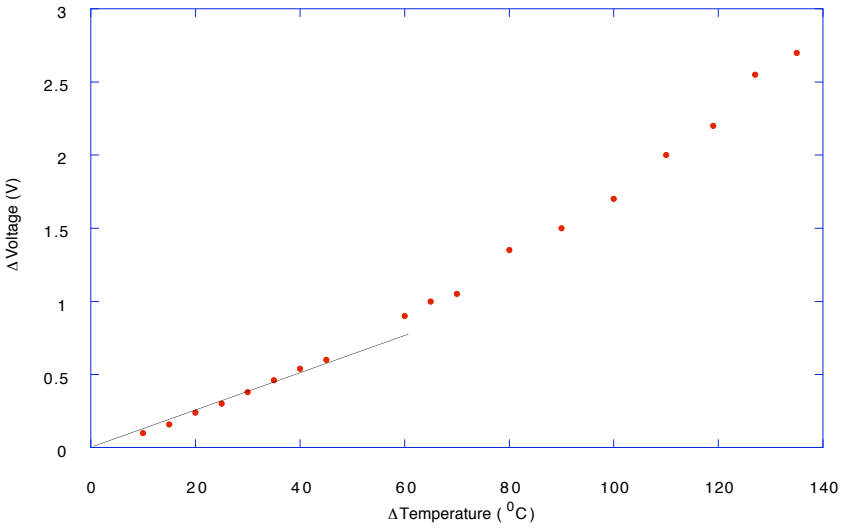

Figure 3.18: Calibration curve of the thermal detector with a 5 mm aperture. Slope of the curve in the linear region is 15 mV/°C.

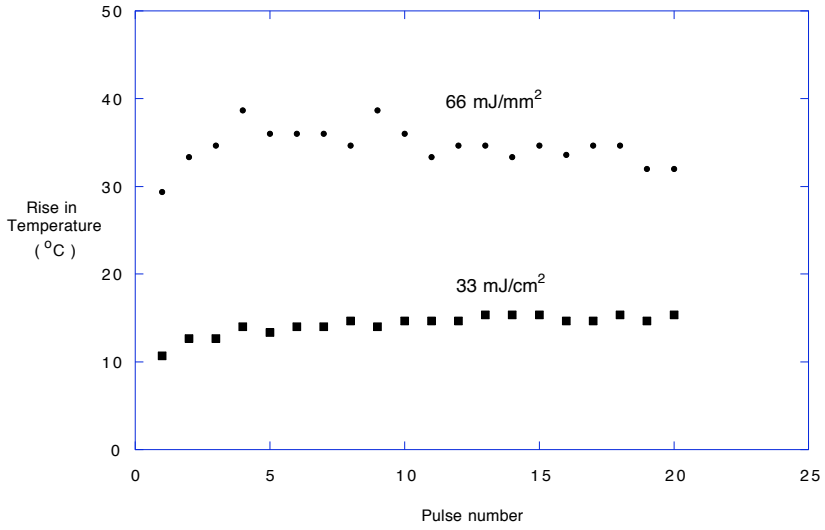

Figure 3.19: Surface temperature rise with each pulse of 33 mJ/mm^2 and 66 mJ/mm^2 on samples stained with 6.45 mM ICG solution. The temperature rise is almost constant with an average rise of 14 ± 1°C and 35±2°C respectively.

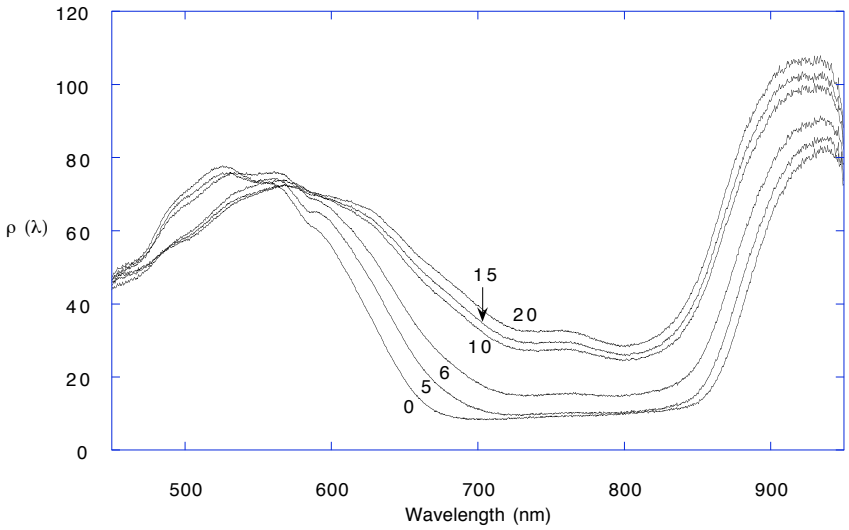

Figure 3.20: Diffuse reflectance measurements of sample irradiated with 33 mJ/mm^2 per pulse for 20 pulses. Only measurements before irradiation and after 5, 6, 10, 15, and 20 pulses are shown for clarity.

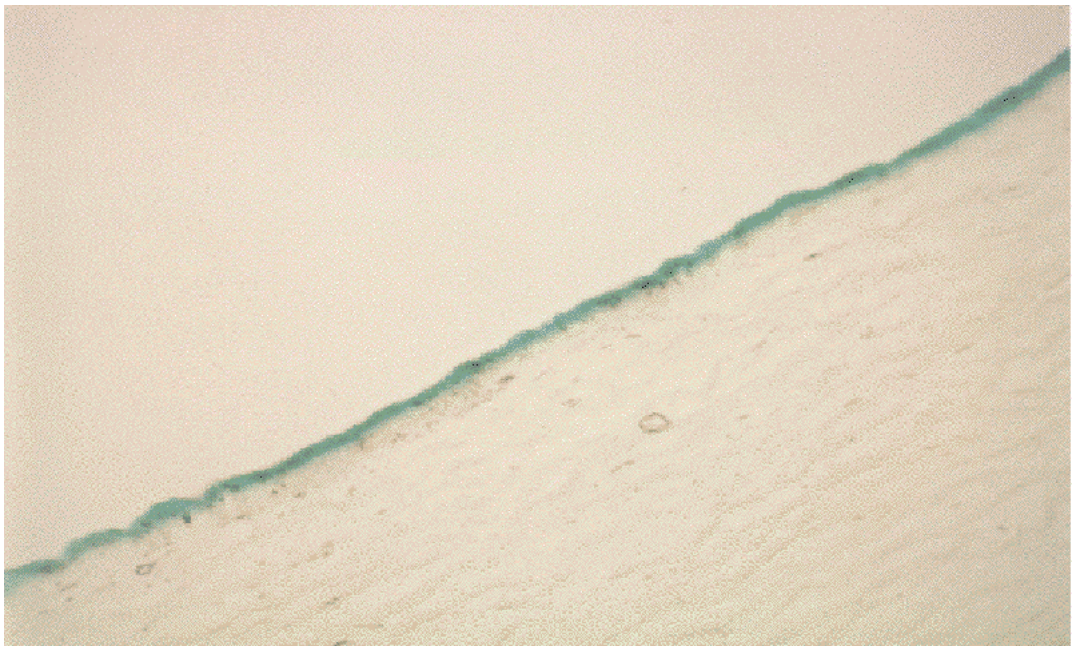

Figure 3.21: The intimal surface of aorta stained with 6.45 mM ICG solution. ICG is absorbed by the tissue and formed a layer of ∼20–30 μm thick in this sample.

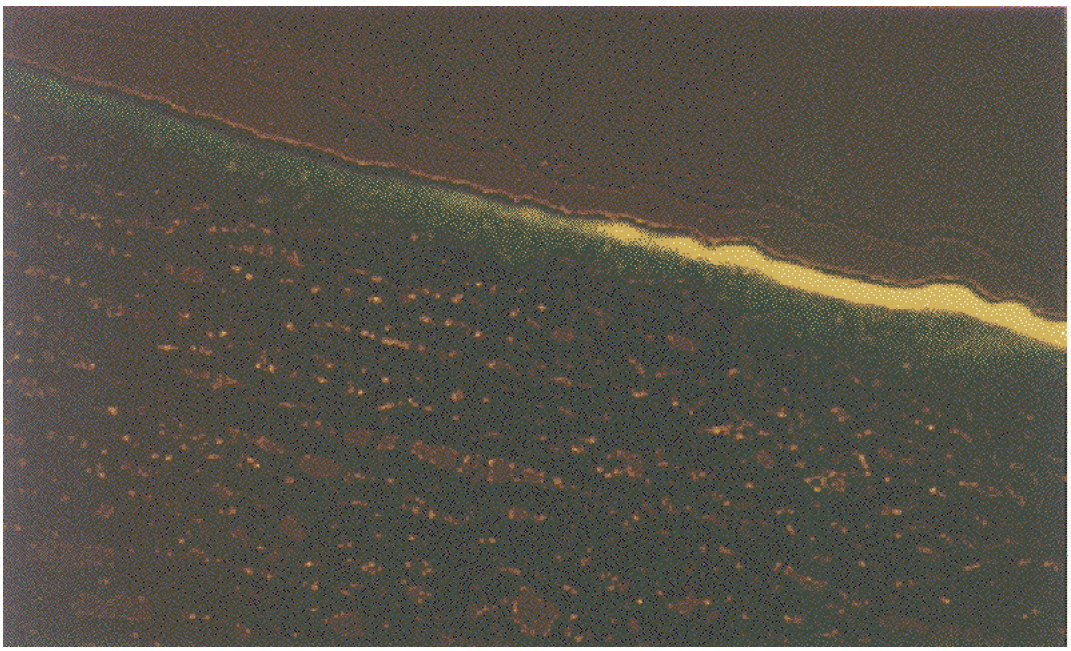

Figure 3.22: The picture shows the contrast between unirradiated control portion on the left and bleached portion on the right. The sample was stained with 6.45 mM ICG solution. The bright fluorescing portion was irradiated with 5 pulses of 55 mJ/mm^2.

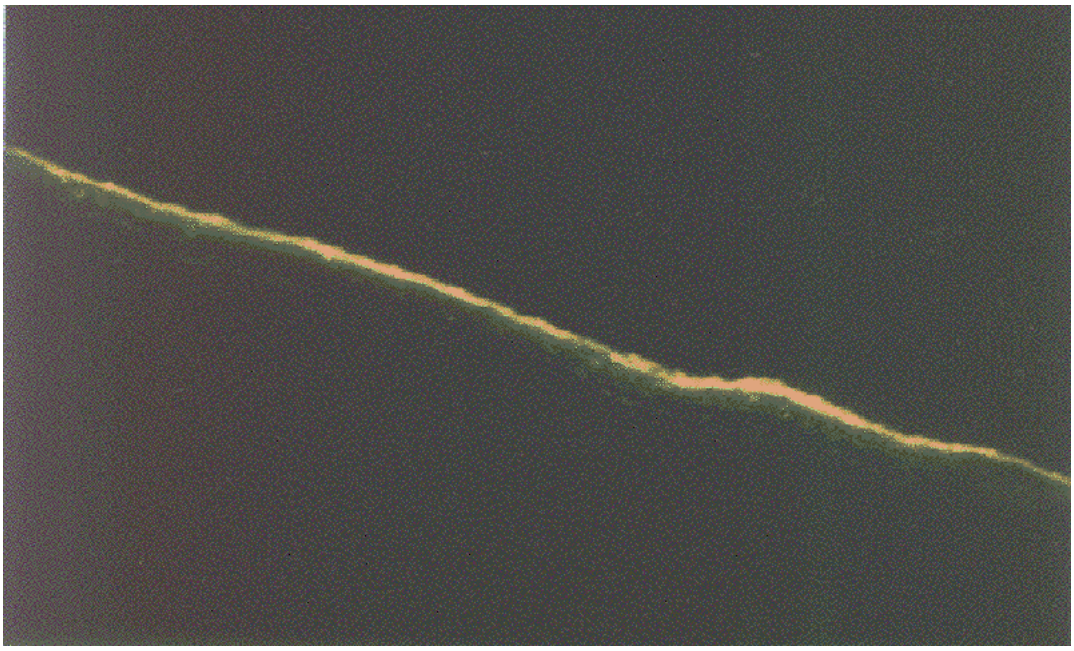

Figure 3.23: Fluorescence of the bleached ICG layer (6.45 mM) after irradiation with one pulse of 55 mJ/mm^2. Thickness of the fluorescing layer was 10 μm.

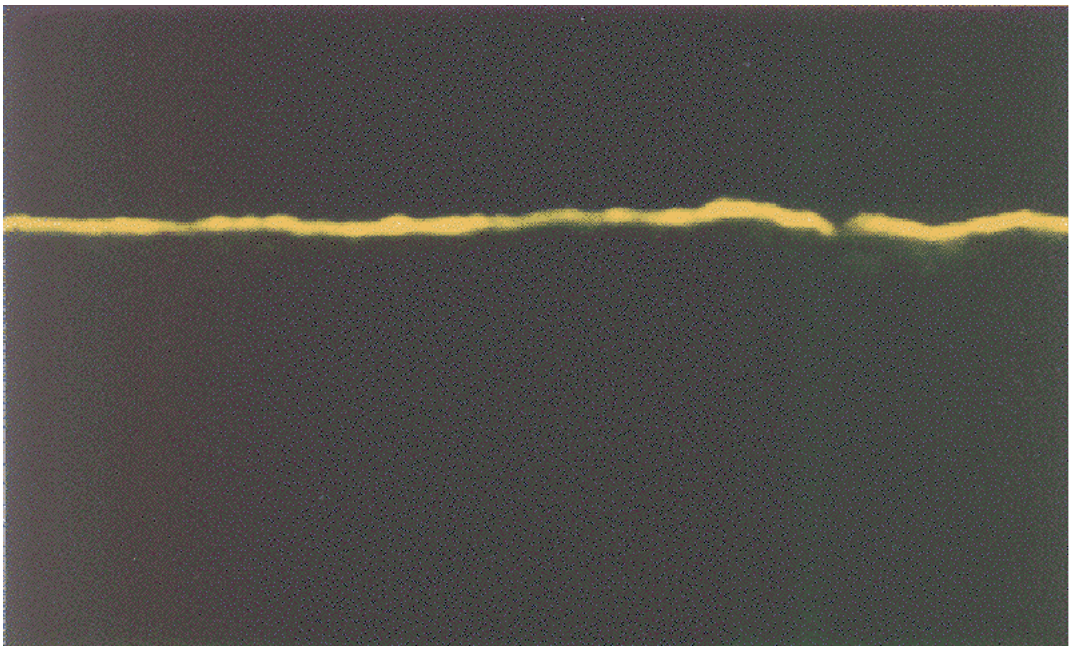

Figure 3.24: Fluorescence of the bleached ICG layer (6.45 mM) after irradiation with 2 pulses of 55 mJ/mm^2. Thickness of the fluorescing layer was 12.5 μm.

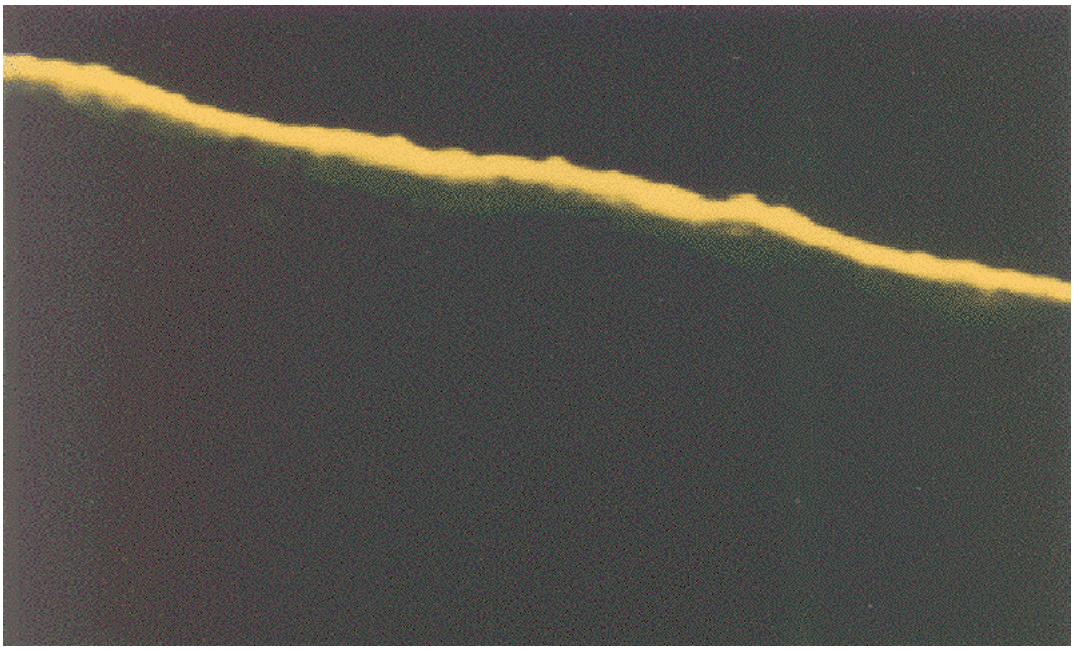

Figure 3.25: Fluorescence of the bleached ICG layer (6.45 mM) after irradiation with 5 pulses of 55 mJ/mm^2. Thickness of the fluorescing layer was 15 μm.

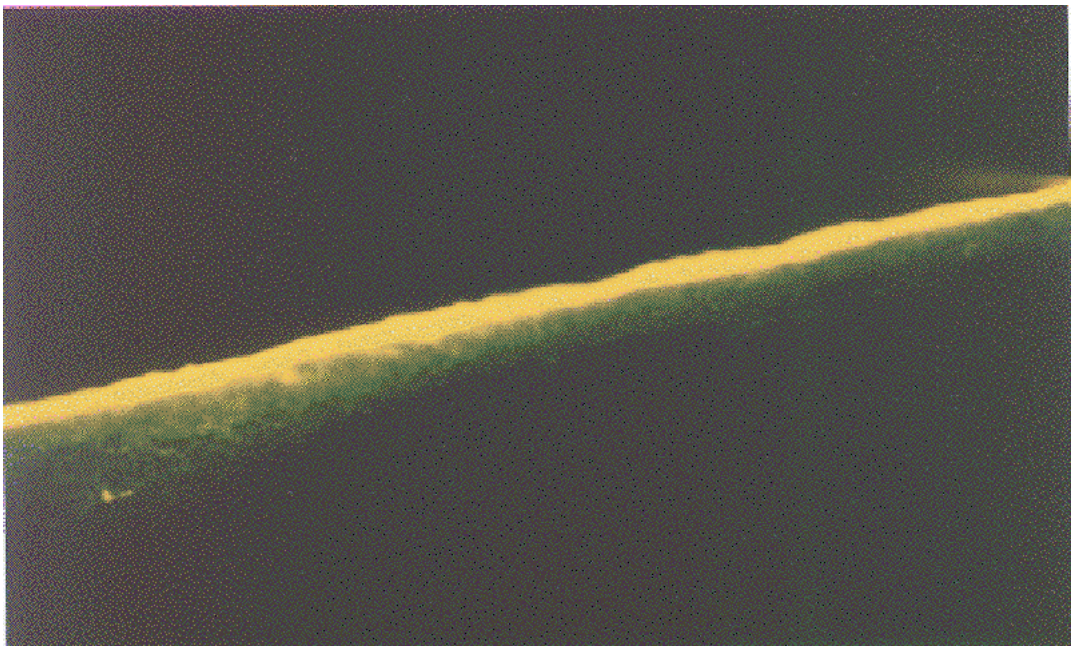

Figure 3.26: Fluorescence of the bleached ICG layer (6.45 mM) after irradiation with 10 pulses of 55 mJ/mm^2. Thickness of the fluorescing layer was 15 μm.

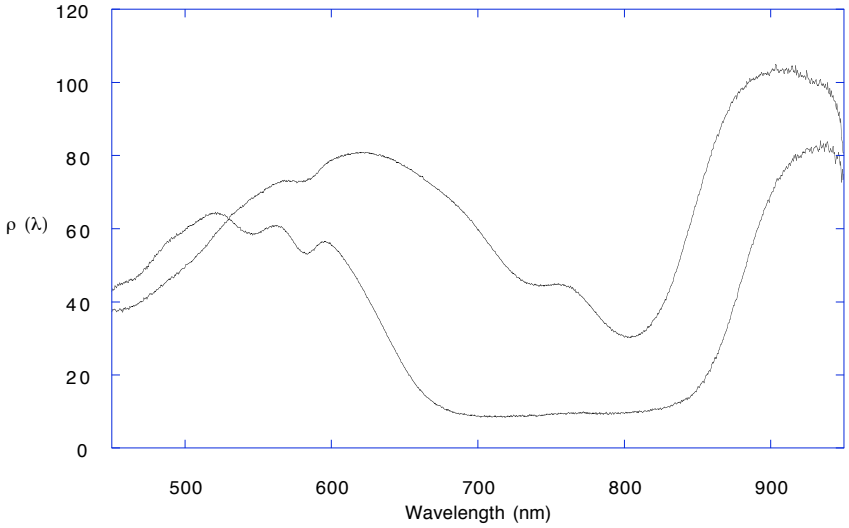

Figure 3.27: Diffuse reflectance measurements of sample irradiated with 66 mJ/mm^2 per pulse for 1 pulse.

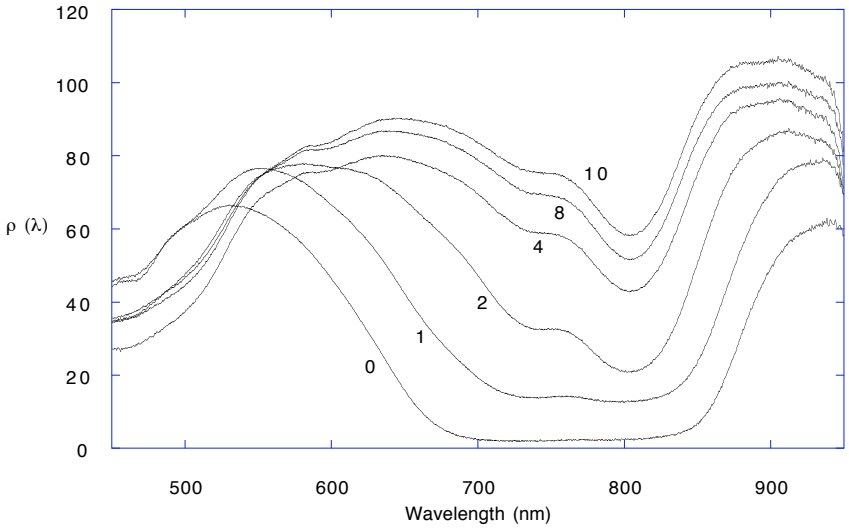

Figure 3.28: Diffuse reflectance measurements of sample irradiated with 66 mJ/mm^2 per pulse for 10 pulse.

Chapter 4

Discussion

In this chapter the observations from reflectance, thermal and, histological measurements are discussed and correlated in terms of ICG degradation with successive laser pulses. The diffuse reflectance data are converted to optical depths using equation 2.4.

4.1 Reflectance Spectroscopy

In the optical measurement system described in section 2.2, one end of the optical fiber bundle was placed in the aluminum holder at an angle of 20° from the normal to the surface (figure 2.2). This was to ensure that no specularly reflected light was collected. Because the intimal surface of aortic tissue is not perfectly smooth, a small amount of diffuse surface reflection may have been collected along with the diffuse backscattered light. This is especially true after multiple laser pulses when the surface becomes dry and flaky. In most reflectance measurements, the baseline measurement is taken with respect to some diffuse reflectance standard such as Spectralon (R = 0.994) and diffuse reflectance is calculated as $R = 0.994(\frac{R_{sample}}{R_{baseline}})$. In the present experimental setup the baseline measurements were made with respect to a glass slide painted white (Krylon acrylic) whose absolute reflectance is unknown. This problem was overcome by measuring the diffuse reflectance of unstained and stained tissue with respect to the same white glass slide. Then, using equations 2.1 and 2.2, the effects due to baseline measurements are cancelled. The true diffuse reflectances of unstained and stained tissues are not known but the reflectance of the stained tissue with respect to that of the unstained tissue is

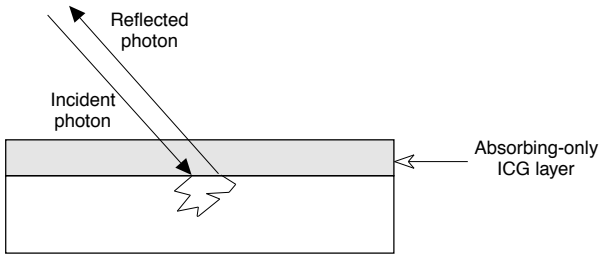

Figure 4.1: The diffusely reflected photon that's detected, is the one that travels back in the same direction as that if the incident photon. This ensures that the photon travels the same thickness of the ICG layer.

known. This is quantity of interest because it can be related to the ICG absorption (equation 2.4).

In equation 2.4, a factor 2 is introduced because light traverses through the thickness of the layer twice. This argument is valid under the assumptions that the ICG layer is absorbing only and the diffusely reflected photons that have large angular deviations from the incident photons are not collected (Figure 4.1). The six collection fibers placed around the illumination fiber collect only those photons reflected back in the same direction as the incident photons. The f-number of the fiber-optic bundle and that of the spectrograph were not matched, but light throughput was maximized by adjusting the distance and height of the fiber bundle at the entrance slit of the spectrograph. This was carried out iteratively by monitoring the halogen lamp spectrum on the OMA.

4.1.1 Variable uptake of ICG

The variation in diffuse reflectance at different positions on stained tissue could be due to non-uniform uptake of ICG by the tissue. The presence of other chromophores, such as blood, may also add to the variation. The presence of blood in varying amounts is evident in Figure 4.2 in which the reflectance measurements of unstained aorta at the proximal and distal ends (from the heart) were made. The blood content at the proximal end of the tissue is more than at the distal end and hence the stronger absorption peaks at 542 nm and 577 nm. This is corroborated by the fact that the aorta is visually more red at the proximal end since it reflects more at higher wavelengths. This variation in diffuse reflection due to blood accounts for less than 10% of the variation in reflection of the ICG layer. Therefore, the diffuse reflection change from site to site could predominantly be due to non-uniform uptake of ICG.

In Figure 4.3 the optical depths calculated using equation 2.4 are plotted for various sites on a stained aorta sample. Figure 3.7 shows the corresponding reflectance spectra. Optical depths are proportional to the temperatures after irradiation, from equation 2.5; different spots on the tissue give rise to different temperatures on irradiation with the same energy. At 800 nm, the wavelength of the diode laser, the optical depth varies at least by a factor of three and hence the final temperature will vary by the same factor. To achieve optimal weld temperatures it may be necessary to vary the incident laser energy accordingly from site to site.

4.1.2 Concentration variation

Bleaching is only observed for samples stained with 3.2 mM and 6.45 mM ICG solution and irradiated with 40 mJ/mm^2. For samples stained with lower concentration bleaching is not observed. Also for radiant exposure of 20 mJ/mm^2, bleaching is negligible or not observed in all the samples. A radiant exposure of 20 mJ/mm^2 is evidently insufficient to cause any significant photothermal or photochemical changes that lead to color changes in the sample. All three samples irradiated with 40 mJ/mm^2 showed a significant increase

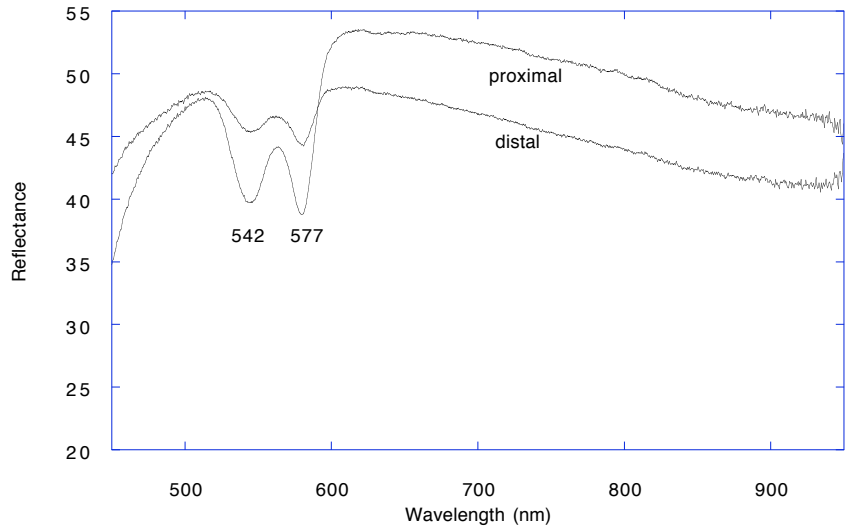

Figure 4.2: Reflectance measurements of unstained aorta at the proximal and distal ends. The stronger absorption peaks due to blood at the proximal end indicate more blood content.

in reflectance with each pulse, and the corresponding decrease in the optical depth is shown in figure 4.4 for the sample stained with 6.45 mM ICG solution. The gradual decrease in optical depth suggests that either the absorption coefficient or the thickness of the ICG layer or both decrease with each pulse.

The decrease in thickness of ICG layer can be visualized as a laser pulse completely bleaching a fraction of the layer. This can happen if the light can only penetrate part of the ICG layer. Earlier transmission experiments show that not all light is absorbed [20]. Additionally, from histological measurements it was seen that the physical thickness and the fluorescing thickness of the ICG layer remained the same (see Figures 3.21, 3.22, 3.23, and 3.24). Therefore, the decrease in optical depth is not due to any decrease in the thickness of the ICG layer but only due to the decrease in the absorption of the layer. The normalized optical depths at 800 nm for all three samples irradiated with 40 mJ/mm^2 are plotted versus pulse number in figure 4.5. The data are normalized to

Table 4.1: The exponents obtained after a power law fit to the optical depth data at 800 nm.

Concentration of ICG (mM)	Exponent
0.8	0.5±0.2
3.2	0.5±0.2
6.4	0.53±0.02

the optical depth of stained ICG layer at 800 nm before irradiation. The points represent experimental data and the line represents a power law fit. In all three samples the optical depths decrease by almost the same power.

The power law can be represented as,

$$\tau = \tau_0 (N+1)^{-\beta} \tag{4.1}$$

where τ_0 is a constant denoting the value at the first pulse and β is a positive number. Table 4.1 tabulates coefficients and the exponents for the 3 samples. With an increase in ICG concentration, facilitating an increased absorption of light one would expect that the decrease in optical depth is faster. But with the data given in table 4.1 it is hard to draw a conclusion. The spectral changes from diffuse reflectance measurements indicate that some form of photochemical changes are taking place that result in molecular structural changes. Photothermal degradation of ICG in albumin is evident from a decrease in optical depth. It is not clear that any degradation by-products are being formed.

In figure 4.6 the optical depth spectra before irradiation of the aorta samples prepared with ICG of 0.8, 1.6, 3.2, and 6.4 mM concentrations are shown. As the concentration increases the absorption bands become flat. The flatness of the absorption bands could be due to two distinct factors. One, it can be interpreted as two unresolved, overlapping bands. We can come to this conclusion from following the spectral shape from lower to higher concentrations. Another factor could be that the absorption is high enough that diffuse surface reflection dominates bulk backscattering [25].

Table 4.2: The exponent in the power law fit to the optical depth data at 800 nm for four different energies.

Radiant Exposure ($\mathrm{mJ/mm^2}$)	Exponent ± 0.1
28	0.4
42	1.0
55	1.4
70	1.8

4.1.3 Energy variation

The optical depth decrease in a sample irradiated with radiant exposures of $28\,\mathrm{mJ/mm^2}$ and stained with 6.45 mM ICG solution is shown in Figure 4.7. It is representative of decrease seen in aorta samples irradiated with higher energies of 42, 55, and $70\,\mathrm{mJ/mm^2}$. The first pulse contributes to the greatest decrease in the optical depth. After 4–5 pulses there is minimal change in optical depth. After 10 pulses a residual ICG signal is still seen.

The normalized optical depths at 800 nm after each pulse for all the above four samples are plotted in Figure 4.8. As expected higher radiant exposures cause faster decreases in optical depth. The exponent is tabulated in Table 4.2.

A linear relationship between the exponent of the power equation and the radiant exposure as seen from Figure 4.9 with a slope of 0.03. From the above observations, it can be said that optical depth τ, is dependent on the number of pulses N, and the radiant exposure Φ. From the linear fit in Figure 4.9, $\beta = 0.034\Phi - 0.49$. Substituting for β in equation 4.1

$$\tau = \tau_0 (N+1)^{-\frac{\Phi - 15}{30}} \tag{4.2}$$

Defining Φ_{th} as the threshold radiant exposure to cause bleaching in the ICG layer and Φ_e as the radiant exposure required for a $1/e$ decrease in optical depth. Then, equation 4.2 can be written as,

$$\tau = \tau_0 (N+1)^{-\frac{\Phi - \Phi_{th}}{\Phi_e}} \tag{4.3}$$

From the above equation and from Figure 4.9, the threshold radiant exposure for any photothermal degradation of ICG layer is about $15\,\mathrm{mJ/mm^2}$.

4.2 Thermal radiometric experiments

For an estimated radiant exposure* of $33\,\mathrm{mJ/mm^2}$ the average temperature rise was $14\pm1^\circ\mathrm{C}$ and for $66\,\mathrm{mJ/mm^2}$ the rise was $35\pm2^\circ\mathrm{C}$. The surface temperature rise increases with incident energy, but is less than what would be expected from reflectance measurements. From figure 4.10, the optical depth before irradiation is 1.15. The thickness of the ICG layer ranges from 15 to $25\,\mu$m and ICG is distributed uniformly over this thickness, then the absorption coefficient μ_a will range from 460 to $770\,\mathrm{cm^{-1}}$. For radiant exposures of $33\,\mathrm{mJ/mm^2}$ and heat capacity $4.2\,\mathrm{J}\ /(\mathrm{g}\,^\circ\mathrm{C})$, temperatures ranging from 360 to 600°C are expected (equation 2.5) if all the absorbed energy is converted to heat. Clearly, the measured temperature rise of 14°C is less than expected.

The reflecting condenser (see figure 2.9) of the diode laser channels the energy from the laser arrays and ideally should produce a uniform square beam at the output end. Because no focusing optics was used at the output aperture, it was found that, a few millimeters away from the aperture the output beam was neither uniform nor square. Only a fraction of the output energy was incident on the spot where the detector was focused and hence a small temperature rise.

If the absorption coefficient is uniform over the thickness of the ICG layer, the decrease in optical depth with successive pulses indicates that temperature jump should also decrease. From figure 3.19, it is seen that the temperature is almost constant for all pulses. This might be possible if heat capacity ϱc, simultaneously decreases with

$$\mu_a$$

. In tissue, heat capacity depends on the amount of water, protein and fat present,

$$c_p = 4.2 m_{water} + 1.09 m_{protein} + 2.3 m_{fat} \qquad (\frac{\mathrm{J}}{\mathrm{g}^\circ\mathrm{C}}) \tag{4.4}$$

*This is an over estimate, see explanation below.

For twenty pulses, water content would need to decrease by 80% to compensate for the decrease in absorption such that temperature remains constant. But such a large decrease in water content is physically unrealistic.

The surface temperatures $T(0,t)$ measured as a function of time were converted to initial temperature distribution $T(z,0)$ as a function of depth using a method by Prahl [26]. The back-calculated initial thermal distribution after the 1, 10, and 20 pulses are plotted in figure 4.11. The temperatures at all depths were normalized to maximum surface temperature. The figure indicates that the maximum temperatures are attained within the first 10–15 μm in the tissue. This suggests that the thickness of the ICG layer is about 10–15 μm in accordance with histological measurements. It is also seen that heat has diffused to a depth of $\sim$50 μm in the 5 ms duration of the laser pulse.

4.3 Histologic assessment

Laser tissue welding is a thermal process. Therefore, understanding heating at the weld site and diffusion of heat to the adjoining area is critical. The optical zone is defined as the depth at which the incident fluence drops by 1/e or 37% [27]. For small pigmented targets, such as a 15 μm ICG layer, the optical zone is specified by the thickness of the pigmented structure. To minimize collateral damage, the pulse duration should be sufficiently short such that heat does not diffuse out of the optical zone. This is known as thermal confinement. A maximum penetration depth of 15 μm requires a pulse duration of less than 1.6 ms to achieve thermal confinement, from the relation

$$t = \frac{d^2}{\kappa} \tag{4.5}$$

where d is the penetration depth and κ is the diffusivity for water is 0.0014 cm^2/s. The pulse length used for these experiments was 5 ms. Therefore thermal confinement was not achieved and some thermal diffusion took place during the laser pulse. This is also evident from Figure 4.11 that heat diffuses for upto 50 μm.

4.4 Understanding spectral changes

The optical depth data for the aorta stained with 6.45 mM ICG solution and irradiated with 10 pulses of 66 mJ/mm^2 each is shown in figure 4.12. It is plotted with respect to wavenumbers because wavenumbers are directly proportional to the photon energy. An absorption spectrum is a superposition of a number of individual absorption bands. The individual bands are described empirically by Gaussian shapes of the form

$$G(\nu) = D \exp\left[-\frac{(\nu - B)^2}{C}\right] \tag{4.6}$$

where ν is the wavenumber in cm^{-1}, D is the amplitude, B is the center, and C is the width of the band. Strictly speaking, absorption bands are Lorentzian in shape, but in a large molecular structure such as tissue protein or ICG, the constant thermal vibrations are averaged over a large number of atomic systems that smear out the band shapes from Lorentzian to Gaussian.

Individual bands can be extracted by fitting to the original spectrum. Through trial-and-error analysis the region from 1700–16000 cm^{-1} was determined to be made up of three individual gaussian bands. Since a Gaussian is characterized by it amplitude, position and width, the problem was to extract these three parameters for all the 10 curves seen in figure 4.12. The spectra were fitted using the Levenberg-Marquardt method of non-linear least square fitting [28]. It was implemented in C language by adapting existing routines for the Marquardt method [29]. Initial guesses for the algorithm were obtained by trial-and-error and the spectrum was fit by χ^2 minimization. Figure 4.13 shows the original spectrum and the three individual bands obtained by fitting. The third band was included to stabilize the fitting algorithm. The center and width of this band fluctuated but the amplitude was consistent with minimal contribution to the whole spectrum. Due to the fluctuating nature of the band center and width, it is not shown with the other bands for clarity. Figures 4.14, 4.15, and 4.16 show the trends in the amplitude, position and width of the bands with each laser pulse.

A decrease in amplitude indicates that photodegradation is taking place. The amplitude of band II decreases much faster than band I. The center of band I shifts to higher

frequency and that of band II shifts to lower frequency. This indicates that there is a change in peak absorption wavelength and suggests some rearrangement of the molecular structure. A similar argument applies to the change in width of the bands. The change in position and width occur only for the first two pulses. The position of band I corresponds to wavelength of the 804 nm diode laser. The chromophore that constitutes band I is primarily responsible for absorption. After absorbing the incident energy the excited chromophore dissipates the energy by participating in a chemical reaction causing bond breaking, crosslinking, or photodestruction of the chromophore itself. It could also thermally dissipate the stored energy by initiating molecular vibrations. Since the chromophore that constitutes band II does not directly participate in absorption, degradation of band II may be due to such photothermal processes.

Figure 4.6 shows optical depth spectra of aorta stained with four different concentrations. Individual absorption bands were also extracted from these spectra. Figures 4.17, 4.18, and 4.19 show the amplitude, position and width characteristics of bands I and II with decreasing concentration of ICG. In figure 4.17, the amplitude of band II drops sharply below 3.2 mM ICG concentration and that of band I decreases steadily. In figure 4.18, the center of band I shifts to a higher frequency and that of band II to a lower frequency. In effect, the band characteristics due to lowering the concentration of ICG are akin to band characteristics due to successive laser pulses. This is expected because photodegradation of ICG with successive laser pulses results in decreased ICG concentration.

4.5 Summary

The realization of an optical fiber-based optical multichannel analyzer facilitated the study of real-time changes in the optical characteristics of stained aorta. The non-invasive system has the potential to monitor laser tissue welding process when used via catheters.

On deriving the optical depths from the reflectance spectra, it is seen that the optical

depth at different spots on the tissue varies at least by a factor of three in aorta after uptake of ICG. The variation in optical depths may be due to non-uniform absorption of ICG by aorta. This means that different temperatures at different spots will be obtained upon irradiation with the same energy. For optimal weld temperatures, the incident laser parameters must be adapted to the optical data.

Visible change in color of the ICG layer from green to orange is manifested in the reflectance spectra as a shift in the absorption peak from 530 to 640 nm. No significant changes in diffuse reflectance is noticed by additional pulses after the ICG layer is bleached. In laser tissue welding ICG is used as the primary light absorber for heat production and when ICG is bleached there should not be any thermal effects at the weld site. Therefore this shift in absorption peak can be used as an indicator to stop the welding procedure.

The decrease in optical depth after each laser pulse that indicates ICG degradation, follows a power law. An increase in the incident energy corresponds to a linear increase in the rate of ICG degradation. An increase in ICG concentration did not seem to increase the rate of ICG degradation due to higher absorption as expected. From the observed data, a threshold radiant exposure of $15\,\mathrm{mJ/mm^2}$ is required to obtain photothermal degradation of ICG and a radiant exposure of $30\,\mathrm{mJ/mm^2}$ is required for a $1/e$ decrease in optical depth. The fact that a clear relationship exists between the optical data and the laser parameters such as number of pulses, incident energy and spot size may aid in achieving reproducible welds.

The temperature rises recorded are much lower than expected. It is possible that thermal diffusion is taking place during the laser pulse as suggested by the calculated initial temperature distributions. Reflectance data suggests that temperatures obtained with successive laser pulses should decrease, but thermal data shows no decrease in temperature. The non-uniformity of the laser beam even at short distances from the condenser renders any accurate temperature measurements difficult. Both thermal and histological measurements indicate that the penetration depth of ICG in aorta is not more than $15\,\mu\mathrm{m}$. This means that thermal confinement is not achieved with a pulse

width of 5 ms. A pulse width of less than 1.6 ms is required for thermal confinement.

Quantification of spectral changes suggest that photochemical and photothermal changes are taking place upon irradiation with light. These changes take place during the first two laser pulses. It is also seen that photodegradation is similar to decreased ICG concentration. It is unlikely that any new by-products are being formed as no new absorption peaks show up.

In this work, a system has been implemented such that real-time monitoring of the laser tissue welding process is possible. A relationship between the optical data and the laser parameters was derived. ICG penetration depth and depth of damage were measured. And finally, the fact that photodegradation of ICG due to successive laser pulses is not only photothermal but also photochemical is realized. The goal of understanding the processes involved in laser tissue welding is achieved here in a limited manner in the hope of bringing the technology closer to reality.

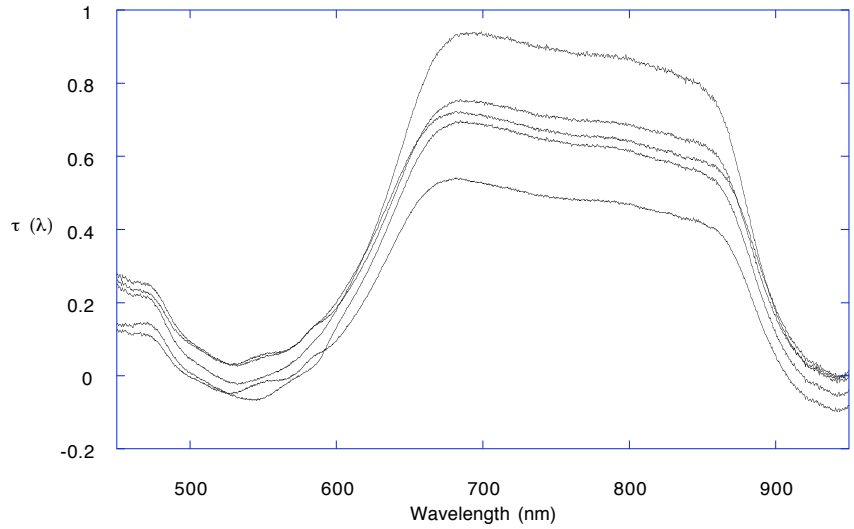

Figure 4.3: The variation in optical depth at various spots on the tissue caused by inhomogeneities in aorta and to some lesser extent by blood content in the tissue. The tissue was stained with 6.45 mM ICG solution.

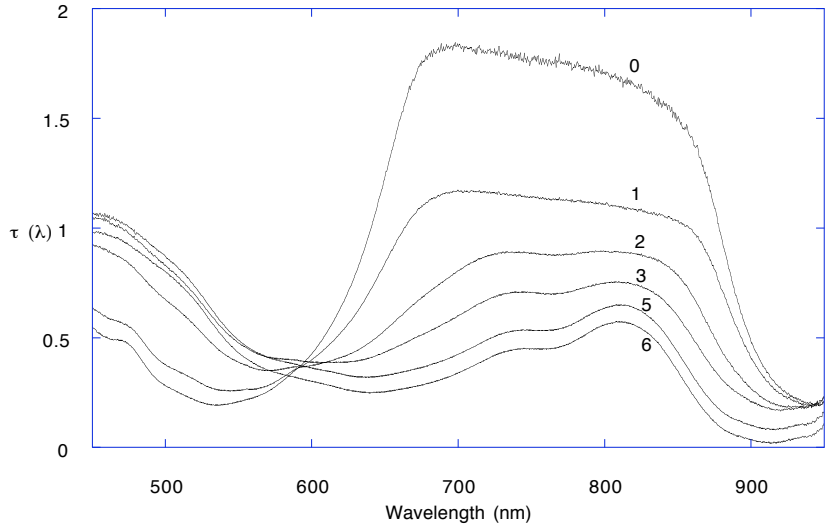

Figure 4.4: Decrease in optical depth with each pulse of 40 mJ/mm^2 for aorta stained with 6.45 mM ICG solution.

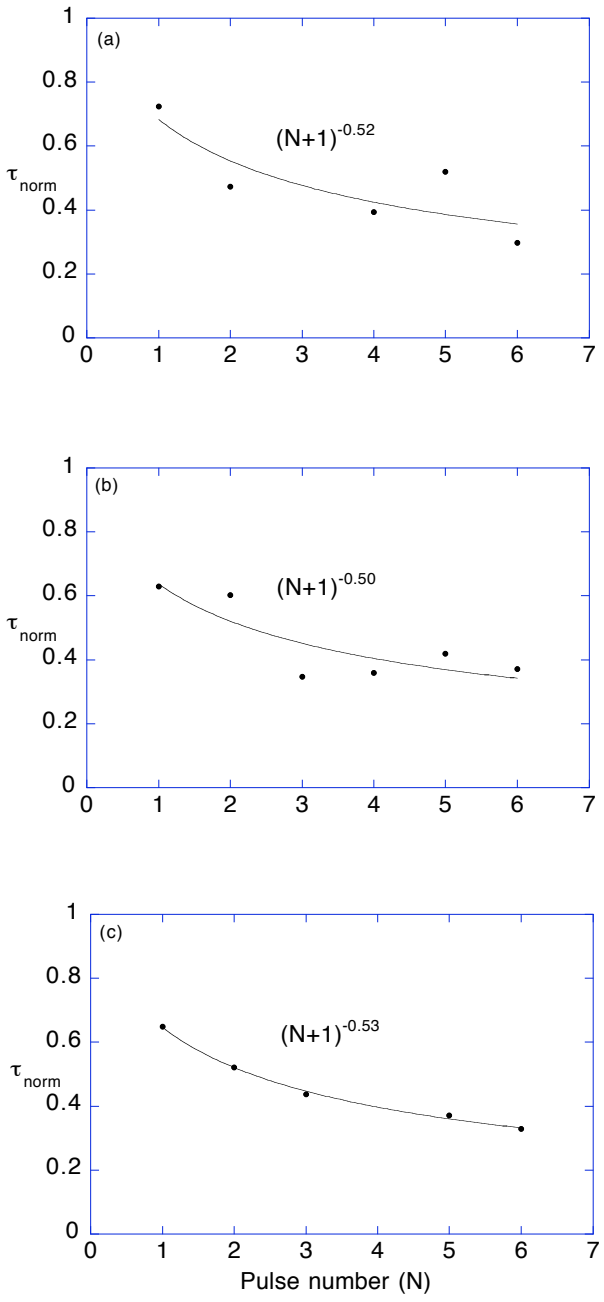

Figure 4.5: The decrease in optical depth at 800 nm follows a power law. The same rate of decrease is observed for ICG concentrations of (a) 6.45 mM, (b) 3.2mM, and (c) 0.8 mM.

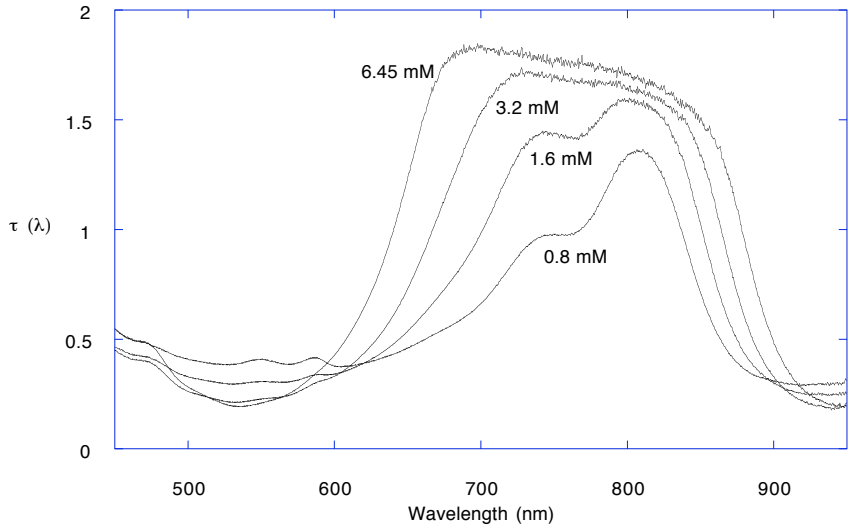

Figure 4.6: Optical depths before irradiation of aorta samples prepared with four different concentrations.

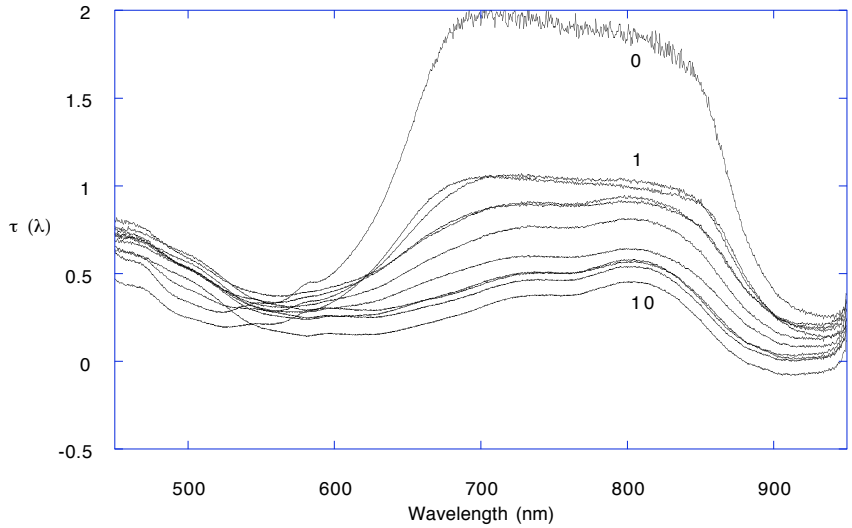

Figure 4.7: Decrease in optical depths with each pulse of 28 mJ/mm^2 for aorta stained with 6.45 mM ICG solution.

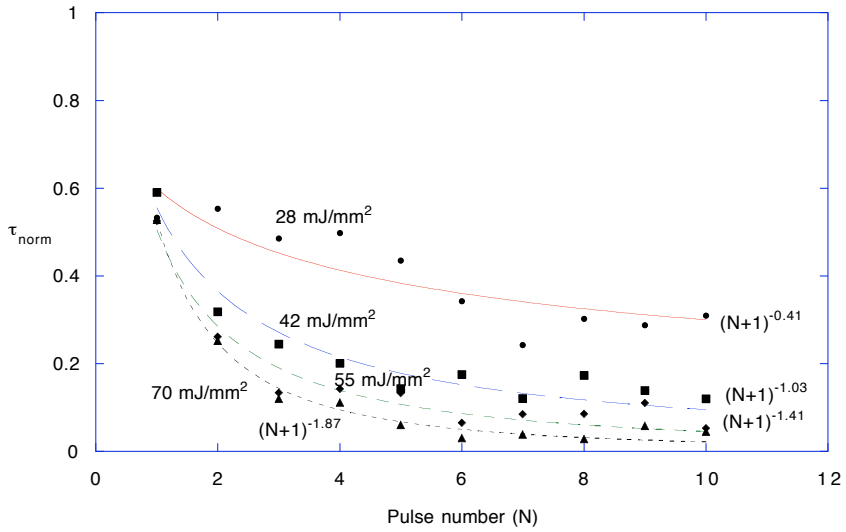

Figure 4.8: The optical depths at 800 nm for four aortas stained with 6.45 mm ICG solution and irradiated with 28, 42, 55, and 70 mJ/mm^2. Solid lines are fitted power law.

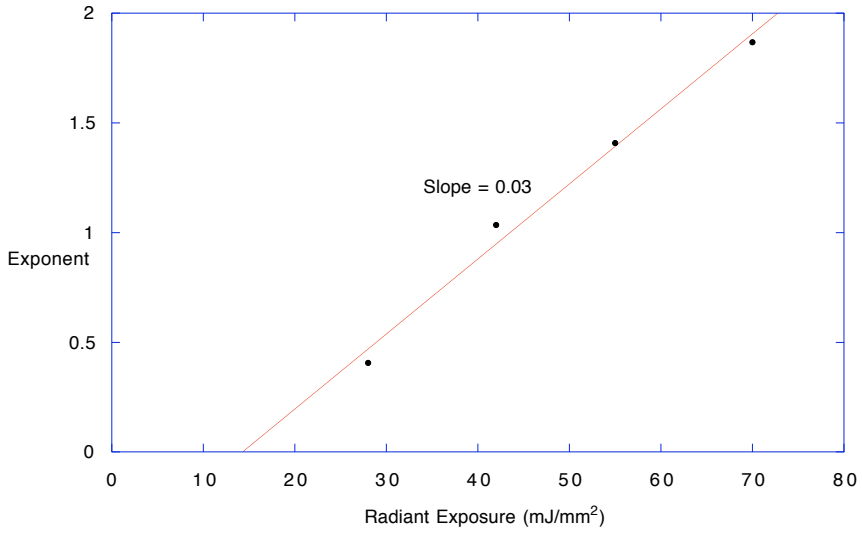

Figure 4.9: The exponent of the power equation increases linearly with energy.

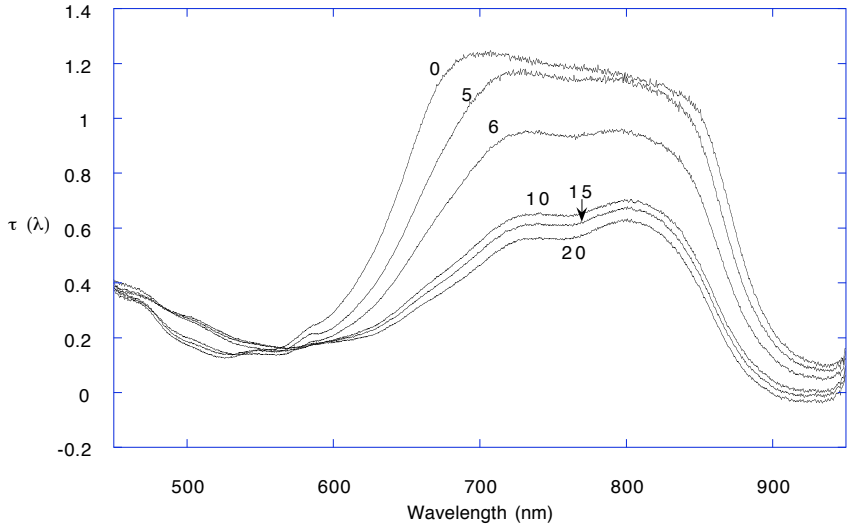

Figure 4.10: The decrease in optical depth with successive pulses of $33\,\mathrm{mJ/mm^2}$.

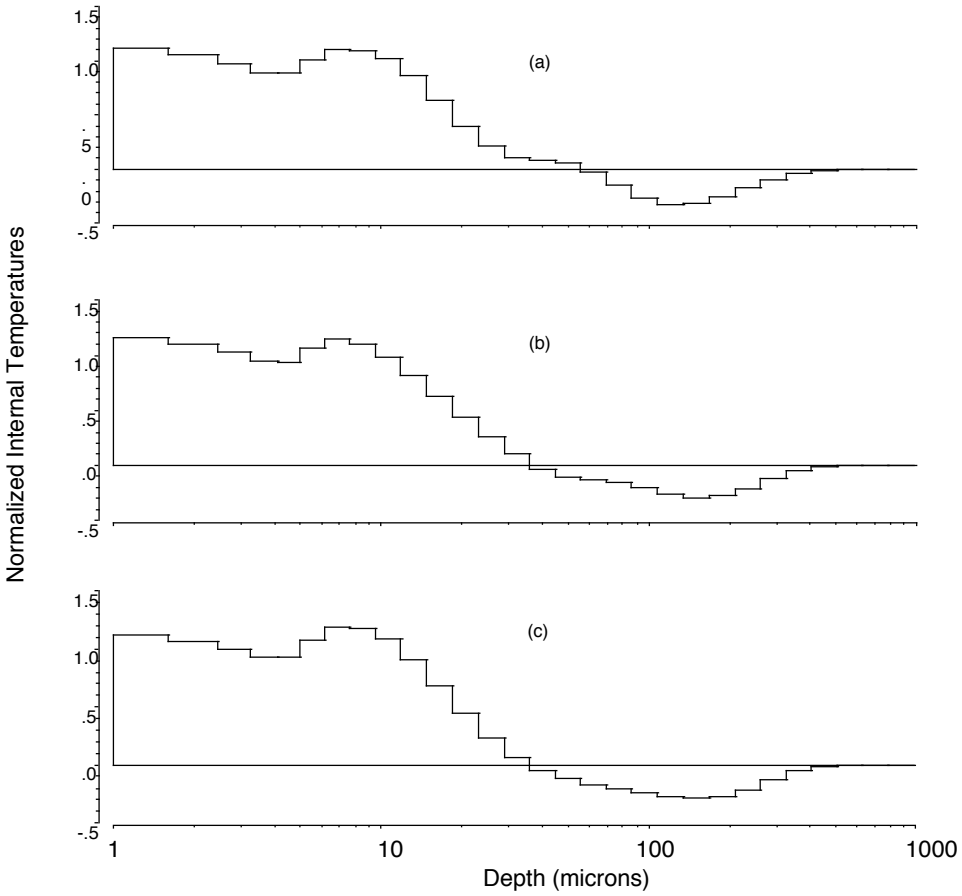

Figure 4.11: Internal temperature profiles of aorta samples irradiated with $33\,\mathrm{mJ/mm^2}$ during the (a) 1^{st}, (b) 10^{th}, and (c) 20^{th} pulse. Maximum temperatures are obtained within a depth of $10\,\mu\mathrm{m}$

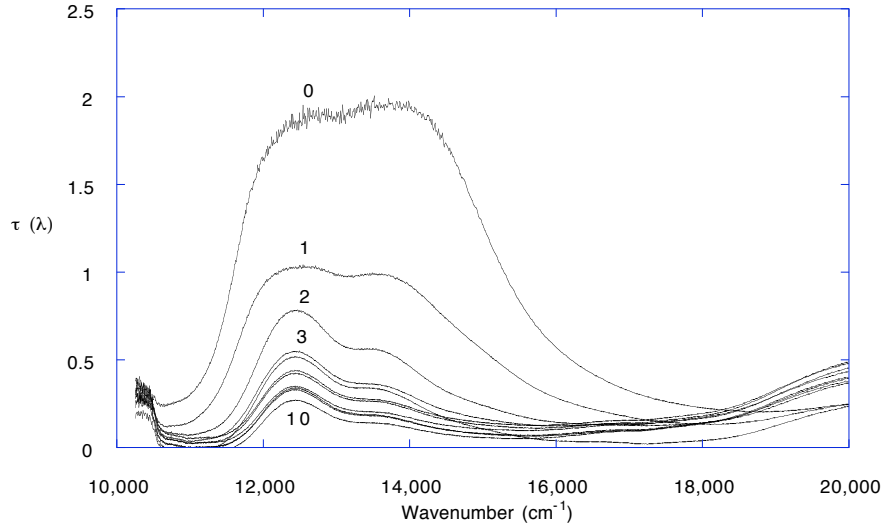

Figure 4.12: Optical depth spectra of aorta stained with 6.45 mM ICG solution and irradiated with 10 pulses of 66 mJ/mm^2 each.

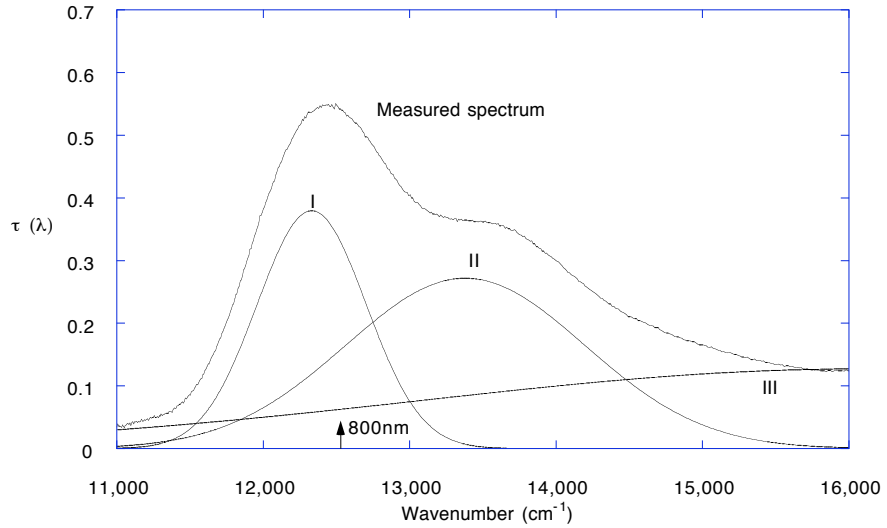

Figure 4.13: Absorption bands of stained aorta after 3 pulses of 66 mJ/mm^2. The lower curves show the spectrum deconvolved into three separate Gaussian bands.

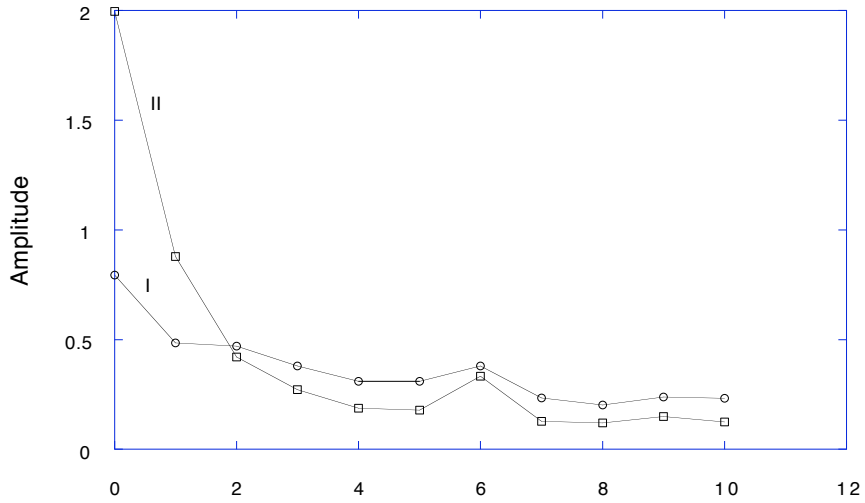

Figure 4.14: The amplitude of the three individual absorption bands as photodegradation takes place. Note that despite the large changes during the first two pulses, both continue to attenuate with successive pulses.

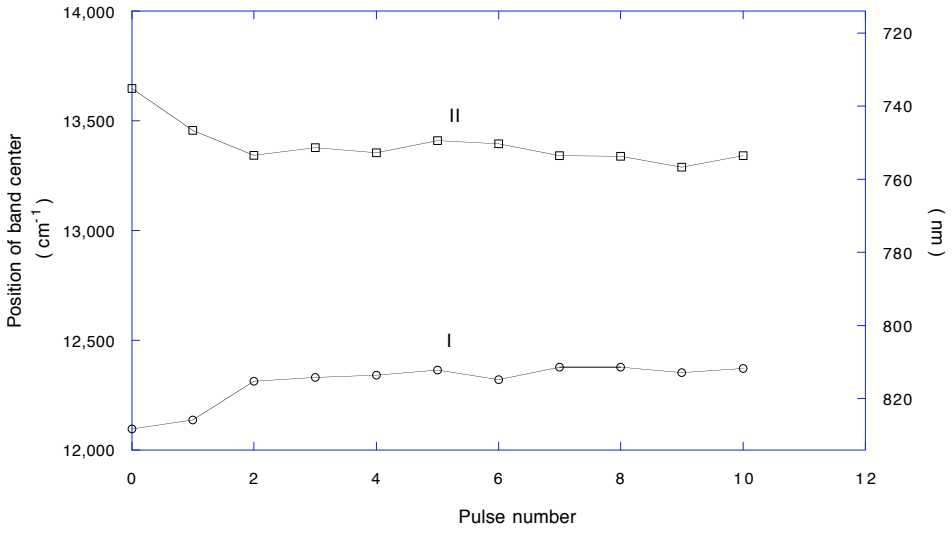

Figure 4.15: The location of the first two absorption bands as a function of pulse number; the center remains constant after two pulses.

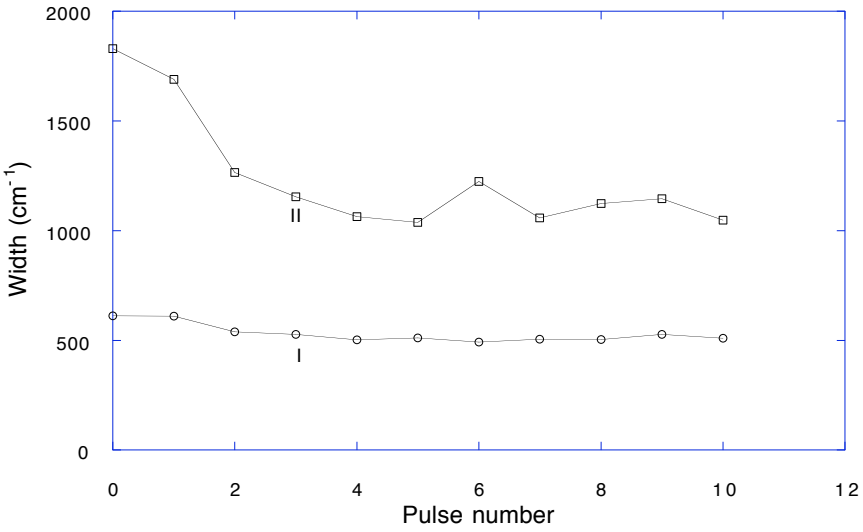

Figure 4.16: The width of the first two individual bands during successive irradiations; the width remains constant after two pulses.

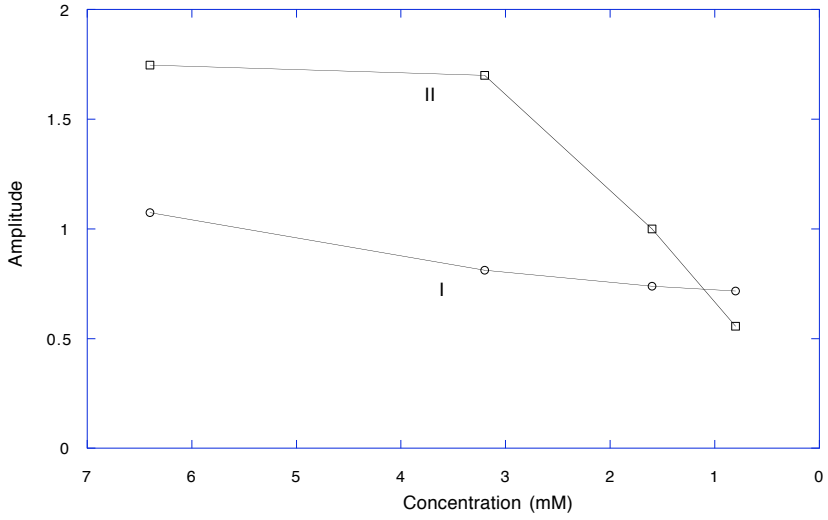

Figure 4.17: The amplitude of the bands as concentration is decreased. The amplitude of each of these bands depends on ICG concentration.

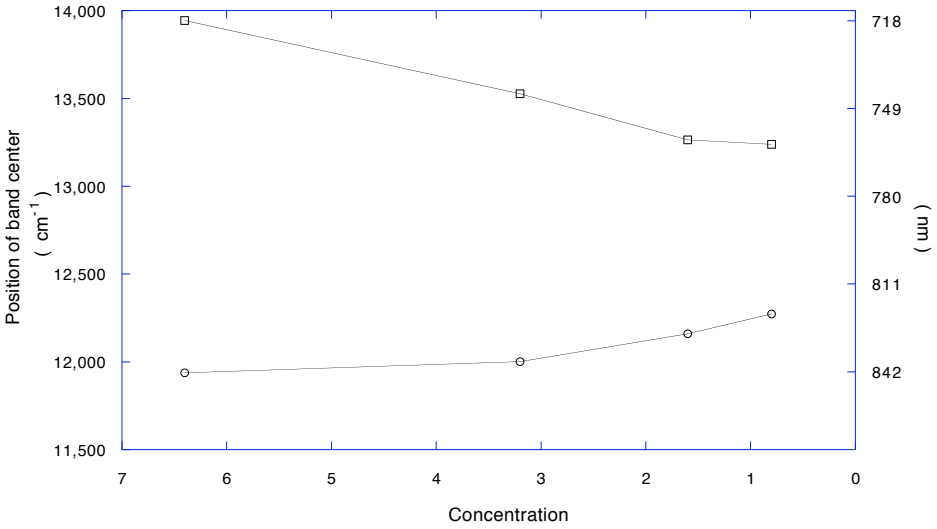

Figure 4.18: The band centers of both absorption bands vary with decreasing concentration.

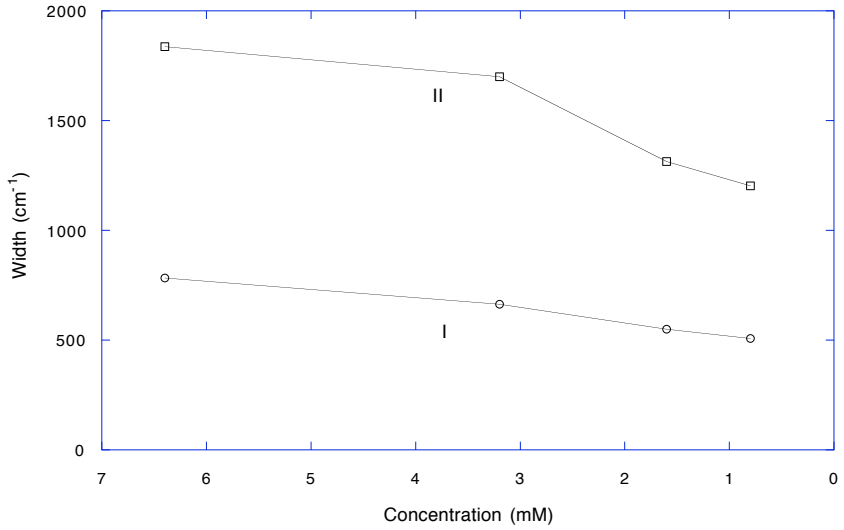

Figure 4.19: The width of the two individual bands narrows with decreasing concentration.

Bibliography

[1] K. J. Strully and W. Z. Yahr, *Micro-Vascular Surgery*, pp. 135–138. Stuttgart: Thieme, 1967.

[2] R. K. Jain, "Transient temperature distributions in an infinite, perfused medium due to a time-dependent, spherical heat source," *J. Biomechanical Engineering*, vol. 101, pp. 82–86, 1979.

[3] S. Thomsen, J. R. Morris, C. R. Neblett, and J. Mueller, "Tissue welding using a low energy microsurgical CO_2 laser," *Med. Instrum.*, vol. 21, pp. 231–237, 1987.

[4] R. A. White, R. P. Abergel, R. Lyons, S. R. Klein, G. Kopchok, R. M. Dwyer, and J. Uitto, "Biological effects of laser welding on vascular healing," *Lasers Surg. Med.*, vol. 6, pp. 137–141, 1986.

[5] S. D. DeCoste, W. Farinelli, T. Flotte, and R. R. Anderson, "Dye-enhanced laser welding for skin closure," *Lasers Surg. Med.*, vol. 12, pp. 25–32, 1992.

[6] J. A. Curcio and C. C. Petty, "The near infrared absorption spectrum of liquid water," *J. Opt. Soc. Am.*, vol. 41, pp. 302–315, 1951.

[7] R. A. White, G. Kopchok, C. Donayre, G. White, R. Lyons, R. Fujitani, S. R. Klein, and J. Uitto, "Argon laser-welded arteriovenous anastomoses," *J. Vasc. Surg.*, vol. 6, pp. 447–453, 1987.

[8] R. A. White, G. H. White, R. M. Fujitani, J. W. Vlassak, C. E. Donayre, G. E. Kopchok, and S. K. Peng, "Initial human evaluation of laser-assisted vascular anastomoses," *J. Vasc. Surg.*, vol. 9, pp. 542–547, 1989.

[9] R. A. White and G. E. Kopchok, "Laser vascular tissue fusion: development, current status, and future perspectives," *J. Clin. Laser Med. Surg.*, pp. 47–54, 1990.

[10] L. S. Bass, M. R. Treat, C. Dzakonski, and S. T. Trokel, "Sutureless microvascular anastomosis using the THC:YAG laser: a preliminary report," *Microsurgery*, vol. 10, pp. 189–193, 1989.

[11] R. Schober, F. Ulrich, T. Sander, H. Durselen, and S. Hessel, "Laser-induced alteration of collagen substructure allows microsurgical tissue welding," *Science*, vol. 232, pp. 1421–1422, 1986.

[12] R. R. Anderson, G. M. Lemole, R. Kaplan, S. Solhpour, N. Michaud, and T. Flotte, "Molecular mechanisms of thermal tissue welding," *Lasers Surg. Med.*, vol. S6, p. 56, 1994.

[13] L. W. Murray, L. Su, G. E. Kopchok, and R. A. White, "Crosslinking of extracellular matrix proteins: a preliminary report on a possible mechanism of argon laser welding," *Lasers Surg. Med.*, vol. 9, pp. 490–496, 1989.

[14] T. F. Helmsworth, C. B. Wright, S. M. Scheffter, D. J. Schlem, and S. J. Keller, "Molecular surgery of th e basement membrane by the argon laser," *Lasers Surg. Med.*, vol. 10, pp. 576–583, 1990.

[15] L. S. Bass, N. Moazami, J. Pocsidio, M. C. Oz, P. LoGerfo, and M. R. Treat, "Changes in Type I collagen following laser welding," *Lasers Surg. Med.*, vol. 12, pp. 500–505, 1992.

[16] F. Barbier and G. A. DeWeerdt, "Chromatography and i. r. spectrography in indocyanine green," *Clin. Chim. Acta*, vol. 10, pp. 549–554, 1964.

[17] M. C. Oz, R. S. Chuck, J. P. Johnson, S. Parangi, L. S. Bass, R. Nowygrod, and M. R. Treat, "Indocyanine green dye-enhanced welding with a diode laser," *Surgical Forum*, vol. 40, pp. 316–318, 1989.

[18] L. S. Bass, S. K. Libutti, and A. M. Eaton, "Tissue bonding and sealing composition and method of using the same," *United States Patent*, vol. 5,209,776, 1993.

[19] L. S. Bass, S. K. Libutti, M. C. Oz, J. Rosen, M. R. Williams, R. Nowygrod, and M. R. Treat, "Canine choledochotomy closure with diode laser-activated fibrinogen solder," *Surgery*, vol. 115, pp. 398–401, 1994.

[20] E. N. La Joie, A. D. Barofsky, K. W. Gregory, and S. A. Prahl, "Welding artificial biomaterial with a pulsed diode laser and indocyanine green," in *Proceedings of Lasers in Surgery: Advanced Characterization, Therapeutics, and Systems V*, vol. 2395, pp. 508–516, SPIE, 1995.

[21] D. H. Sliney, "Deriving exposure limits," in *Proceedings of Laser Safety, Eyesafe Laser Systems, and Laser Eye Protection*, vol. 1207, pp. 2–13, SPIE, 1990.

[22] M. L. J. Landsman, G. Kwant, G. A. Mook, and W. G. Zijlstra, "Light-absorbing properties, stability, and spectral stabilization of indocyanine green," *J. Appl. Physiol.*, vol. 40, pp. 575–583, 1976.

[23] S. A. Prahl, I. A. Vitkin, U. Bruggemann, B. C. Wilson, and R. R. Anderson, "Determination of optical properties of turbid media using pulsed photothermal radiometry," *Phys. Med. Biol.*, vol. 37, pp. 1203–1217, 1992.

[24] S. L. Jacques, J. S. Nelson, W. H. Wright, and T. E. Milner, "Pulsed photothermal radiometry of port-wine-stain lesions," *Appl. Opt.*, vol. 32, pp. 2439–2446, 1993.

[25] B. Hapke, *Theory of Reflectance and Emittance Spectroscopy*. Cambridge University Press, 1993.

[26] S. A. Prahl, "Pulsed photothermal radiometry of inhomogeneous tissue," in *Progress in Photothermal and Photoacoustic Science and Technology* (A. Mandelis and P. Hess, eds.), AIP Press, (in press).

[27] S. L. Jacques, "Role of tissue optics and pulse duration on tissue effects during high-power laser irradiation," *Appl. Opt.*, vol. 32, pp. 2447–2454, 1993.

[28] P. R. Bevington and D. K. Robinson, *Data Reduction and Error Analysis for the Physical Sciences*. McGraw-Hill, 1992.

[29] W. H. Press, B. P. Flannery, S. A. Teukolsky, and W. T. Vetterling, *Numerical Recipes: The Art of Scientific Computing*. Cambridge University Press, 1986.

Biographical Note

Krishna Kumar was born in Hyderabad, India on February 5, 1968. He attended Wichita State University and earned an M. S. degree in Physics. His present interests are in biomedical optics and biomechanics.